DESIGN AND FABRICATION OF MAGNETIC PDMS NANOCOMPOSITE USING IRON OXIDE NANOPARTICLES

by

Benjamin Dopphoopha

A Thesis Submitted in Partial Fulfillment of the Requirements for the Degree of
Master of Engineering in Nanotechnology

Examination Committee:	Dr. Tanujjal Bora (Chairperson)
	Prof. Manukid Parnickhun
	Dr. Bhawat Traipattanakul

Nationality:	Thai
Previous Degree:	Bachelor of Engineering in Mechanical Engineering
	Chiang Mai University
	Thailand
Scholarship Donor:	His Majesty the King's Scholarships (Thailand)

Asian Institute of Technology
School of Engineering and Technology
Thailand
May 2021

AUTHOR'S DECLARATION

I, Benjamin Dopphoopha, declare that the research work carried out for this thesis was in accordance with the regulations of the Asian Institute of Technology. The work presented in it are my own and has been generated by me as the result of my own original research, and if external sources were used, such sources have been cited. It is original and has not been submitted to any other institution to obtain another degree or qualification. This is a true copy of the thesis, including final revisions.

Date:

Name: Benjamin Dopphoopha

Signature:

ACKNOWLEDGMENTS

ABSTRACT

Soft materials can be found all over the world. Not only can they be found in man-made items, but nature also utilized soft materials such as leaves, muscle, organs, and more. Seeing nature as inspiration, soft materials became the focus of research around the world. Soft materials have the advantage of having many degrees of freedom compared to hard materials. This advantage also comes with its disadvantages as having a high degree of freedom also leads to complex control systems. To resolve this, there are research that aims to develop methods to manipulate soft materials and utilize them. In this study we have fabricated a soft structure based on magnetic Polydimethylsiloxane (PDMS) nanocomposite material. PDMS is a biocompatible polymer material which was modified with magnetic Fe_3O_4 nanoparticles to make it magnetic in nature. The nanoparticles were characterized by using electron microscopy and x-ray powder diffraction to study the morphological and material properties of the nanoparticles. The nanocomposite was then characterized to understand its mechanical strength using texture analysis testing machine. By controlling the quantity and alignment of the magnetic domains within the nanocomposite, we have made a structure and demonstrated its movement by applying an external magnetic field.

CONTENTS

LIST OF TABLES

LIST OF FIGURES

LIST OF ABBREVIATIONS

PDMS   = Polydimethylsiloxane

Fe   = Iron

Fe_3O_4 = Iron (II, III) Oxide or Magnetite

GC   = Graphite Carbon

PAE   = Phthalates Esters

MRI   = Magnetic Resonance Imaging

DEA   = Dielectric Elastomeric Actuators

SMA   = Shape Memory Alloys

CI   = Carbonyl Iron

CNP   = Carbon Nanoparticles

TEM   = Transmitted Electron Microscope

HRTEM   = High Resolution Transmitted Electron Microscope

SAED   = Single Atom Electron Diffraction

XRD   = X-ray Powder Diffraction

ICDD   = The International Center for Diffraction Data

A   = Amperes

T   = Tesla

FFT   = Fast Fourier Transform

CHAPTER 1
INTRODUCTION

1.1 Background of the Study

Soft materials are ubiquitous around the world. Examples of soft materials can be found in nature such as leaves, plant fibers, or even the muscles of living animals. Soft materials are also used in everyday applications like packaging materials, foams, and rubber tires. Soft materials are very significant because of their many properties, such as their flexible nature and deformation behavior, and significant research across the world to study about soft materials and how they can be used in different applications in currently ongoing.

One advantage of soft materials is the high degree-of-freedom in terms of their movement which is beneficial in many applications, such as soft robotics. What traditional robots have in common is a rigid structure and fixed amount of degree of freedom. These properties are good because they allow robots to do the same task multiple times, and they allow great accuracy when performing these tasks. However, these rigid robots do not function efficiently outside of their working environment.

Soft robotics is an emerging field of robotics that uses soft and compliant materials in all or part of the robots. Soft robotics emerged starting inspiration when observing nature. Many animals have soft bodies, and they exploit these bodies to the fullest. The ways that these animals take advantage of their bodies are squeezing through tight spaces, hiding to ambush prey, grabbing objects and more. There are also animals that may not be soft-bodied but have a soft body part that helps them to tackle problems and go through their daily lives.

Another application of soft materials is in the biomedical field. Living beings including animals, humans, and plants consist of soft materials. Muscles are soft materials that can contract or relax to perform movements for animals such as walking, running, grabbing, and climbing. Organs are soft materials that exist in living bodies that perform different functions for the body to survive and live. The heart pumps blood to deliver oxygen for the other organs. The lungs expand and contract to breathe in air to provide.

The biomedical field involves these Applications of soft materials in the biomedical field include artificial muscles or organs, prosthetics that function like real limbs, and micropumps that uses soft materials to pump liquids at the rate of the microscale by actuation. Soft materials can also be applied in this field to help perform surgery or to help diagnosis the illness by investigating inside the body.

Although there are many advantages of soft material, there are also limitations that comes with them in their respective field that they are being applied. Soft materials have greater degrees of freedom than rigid materials which means they can bend more freely. This can lead to problems if the material is left unchecked such as bending uncontrollably and easily bending to minimal force. These problems can cause complications to soft robots. Increased degree of freedom makes it harder to control the robot. Because of this, different methods are used to control the movement of the soft robots. These methods include air compression, expanding materials when heated, and more. Though there are various methods that are utilized, each method has their own disadvantages including using a large of amount of energy to maneuver, damaging of the material used to control the structure, and needing an independent source of fluid to control the structure.

Limitations of soft matter also occurs in biomedical field. Much research involves finding ways to actuate the materials to mimic organs. Mimicking the movement of organs almost perfectly is crucial for artificial muscles or organs to work with the human body. The materials to be used must be able to harden or tense up whenever needed such as when a muscle is contracting. The choice of the material is also important because the material needs to be biocompatible for the human body to accommodate whatever structure that is in it. The material was be chosen carefully since the human body is very sensitive to foreign bodies and materials.

In this study, a concept that utilizes nanotechnology to prepare a soft material is tested. The study involves developing a magnetic flexible thin structure that would be controlled externally by a magnetic field source. The magnetic structure will be made with a polymer and magnetic nanoparticles dispersed through the polymer. In concept, the flexible polymer structure will be tested by being placed at a set distance to a magnetic source. The interaction of the structure will then be analyzed.

1.2 Statement of the Problem

Rigid structures are great for applications that require strength and long-lasting durability. However, these materials are at risk of not able to adapt to different situations or cannot be used where higher degrees of freedom are desired. Because of soft materials have a continuum deformation of their flexible nature which gives them high degree of freedom, methods are needed to be developed to control their properties and their behavior. Current ways of achieving this have their limitations. These limitations can include using a large of amount of energy to maneuver, damaging of the material used to control the structure, and needing an independent source of fluid to control the structure.

1.3 Research Questions

The research questions that this thesis is aimed to answer are shown below:

1. How does varying the magnetic field affect the movement of the structure?
2. How does concentration of iron oxide nanoparticles affect the performance of the structure?
3. Can alignment improvement the performance of the magnetic structure?

1.4 Objectives of the Study

1. To develop a magnetic soft structure using magnetic nanoparticles incorporated in polydimethylsiloxane (PDMS) polymer that is flexible and can be deflected using an external magnetic field.
2. To characterize the nanoparticles to analyze the morphological and material properties, and to evaluate the structural integrity and mechanical strength of the magnetic soft structure.
3. To evaluate and demonstrate the movements of the magnetic soft structure under the influence of an externally applied magnetic field and investigate the movement with respect to the concentrations of the magnetic nanoparticles.

1.5 Scope

1. Structure will be made with polydimethylsiloxane (PDMS) and iron oxide nanoparticles.
2. Iron oxide nanoparticles are synthesized by co-precipitation method.

CHAPTER 2
LITERATURE REVIEW

Chapter 2 will go over some literature to give some background in this study. This chapter will first start by explaining what magnetic nanoparticles are and what types of magnetic nanoparticles are there. Then the chapter will introduce some methods on how to synthesize iron oxide nanoparticles and the applications of iron oxide nanoparticles. Then, the chapter will focus on magnetic soft materials and their application in different fields.

2.1 Magnetic Nanoparticles

Magnetic nanoparticles are nanoparticles that can be controlled by a magnetic field. These particles are usually at in the range of 1 to 100 nm in size while particles bigger than these are considered microparticles. Nanomaterials exhibit different properties from their bulk counterparts such as chemical properties, optical properties, electrical properties, and more. Magnetic materials in the nanoscale are no different as decreasing their size also affects their magnetic properties.

Magnetism is a phenomenon that is caused by the magnetic moment of electric charge which is caused by the motion of electric charge. This results in attractive and repulsive forces between objects like magnets attracting magnets or electromagnets attracting metal objects. The motion of electric charge usually occurs when the electrons orbiting the atoms. A current are electrons in motion so current will also produce a magnetic field which electromagnet make use of.

Types of magnetism:

- **Paramagnetism**

  Paramagnetism is a form of magnetism where materials have a weak attraction to externally applied magnetic field. Each atom of the material has its own magnet moment and are randomly oriented. When a magnetic field is applied to the material, the magnet moments will rotate to align to the field.

- **Ferromagnetism**

  Materials that exhibit strong magnetic properties are usually ferromagnetic. They contain atoms that have permanent magnetic moments that have a tendency to align parallel to each other even in a weak magnetic field. This type of magnetism is the strongest and can be seen with normal magnets that are used in households.

- **Superparamagnetism**

  Materials that are in the nanoscale have different magnetic properties than their bulk counterparts. Superparamagnetism is a form of magnetism that occurs in small ferromagnetic nanoparticles. Ferromagnetic materials have domains that are areas of the material have magnetic moments that points in the same direction. Superparamagnetism involves the nanoparticles have a single magnetic domain due to their size. This occurs in when nanoparticles' diameters are within the range of 3 to 50 nm.

There are two types of magnetic nanoparticles that are either made of hard or soft magnetic materials. What determines a material to be a hard or soft magnet depends on the strength of the magnetic field needed for alignment of magnetic domains which is called coercivity (*6.9: Hard and Soft Magnets - Chemistry LibreTexts*, n.d.). Hard magnets have high values of coercivity, so they retain magnetization even without a magnetic field. Soft magnets have low values of coercivity, so they lose their magnetization once the magnetic field is gone.

Soft magnetic nanoparticles are usually occupied by oxides or ferrites. There are many ferrite nanoparticles but the most explored in this category is iron oxide nanoparticles that either come in the form of maghemite or magnetite. When these nanoparticles are small enough, they exhibit superparamagnetic properties. Since they are soft magnetic nanoparticles, their remanence goes to zero when there is no magnetic field.

Hard magnetic nanoparticles are able to be magnetized after the source of magnetic field is removed due to their coercivity is high compared to soft magnetic nanoparticles. This gives them an advantage over soft magnetic nanoparticles in terms of magnetic tuning and aligning. However, while it is true that they are hard to be demagnetized it

is also true that they are hard to get magnetized, so a strong external magnetic field is needed (Mody et al., 2013).

There are many magnetic nanoparticles but in this study iron oxide nanoparticles will be the focus since these will be the main material for this study in the project.

2.1.1 Synthesis of Magnetic Iron Oxide Nanoparticles

There are many methods to synthesis magnetic iron oxide each with their advantages and disadvantages which are normally classified as top-bottom and bottom-up methods. These methods usually involving physical methods such as ball milling (Jalil et al., 2017) and chemical methods. In research, bottom-up methods are usually prefered over top-bottom methods because of better control of the results even though bottom-up methods are shown to be slower and have lower yields. This type of method encompasses many methods.

Co-precipitation method is the most used method to synthesis iron oxide nanoparticles. The method is relatively straight forward and can be done in a room temperature setting (Anbarasu et al., 2015; Wulandari et al., 2018). This method involves adding a base at a certain rate to a Fe^{2+}/Fe^{3+} salt solution to make the environment alkaline to grow Fe_3O_4 nanoparticles (Liu et al., 2020). Due to the resources available in this study, this method will be used for the synthesis of this project.

The hydrothermal method is a method that involves a reaction medium that consist of an aqueous solution in a sealed reactor (Liu et al., 2020). High temperature and pressure are set in the reactor by setting external conditions that can dissolve insoluble substances. The product from this reaction is then recrystallized, and then separated to go through heat treatment to obtain nanoparticles. This method provides good magnetic properties due to the high-temperature environment and can achieve good purity of the product.

The pyrolysis method uses high temperatures to thermally decompose metal compounds. After this, the precursor is then oxidized to produce magnetic metal oxide nanoparticles. The results obtained are magnetic nanoparticles that are uniform in size

and shape, crystalline, isolated, and have high values of saturation magnetic susceptibility and initial magnetic susceptibility (Liu et al., 2020).

2.1.2 Applications of Magnetic Iron Oxide Nanoparticles

Due to the properties of iron oxide nanoparticles, research also focuses on using them in a wide range of applications. These applications include wastewater treatment, food analysis, and the medical science.

One of the world's problem is wastewater, so wastewater treatment is in high demand to be developed by using various methods. Because of the properties of magnetic nanoparticles such as magnetism and repeatability, research has begun focusing on using these nanoparticles. Iron oxide nanoparticles with mordenite were prepared to be used for treating oily wastewater (Hesas et al., 2019). This method allowed that nanoparticles to be used five times continuously to purify petroleum waste.

Another application for iron oxide nanoparticles is food analysis due consumers being more conscious about food safety and government departments formulating laws and regulations on food safety. Because of this, food needs be accurately and effectively analyzed to get test results that can be effectively used. To achieve this, magnetic nanoparticles are used to detect substances like bacterial pathogens, banned food additives and more. Fe_3O_4@GC was prepared and effectively used for separating and analyzing five phthalates acid salt (PAE) which are used in food packaging (Tong et al., 2019).

Magnetic nanoparticles are also used in medical science. In fact, research has be using nanotechnology in medical sciences (Sousa et al., 2019). Examples of this are targeted drug delivery (Shen et al., 2018), biosensors, magnetic resonance imaging (MRI) and more. Due to their magnetic properties, tumor diagnosis and treatment can be improved, and patients can suffer less side effect. Magnetic nanoparticles can also be used for tissue engineering to heal damage in the body or grow new organs (Liu et al., 2020).

2.2 Soft Materials

Soft materials have a range of advantages over hard materials depending on the material such as flexible and greater degree of freedom. However, these advantages can also become a disadvantage if leave unchecked. Flexibility and greater degree of freedom also means that the material is harder to control. Because of this, there is research that is focused on founding developing methods to control soft materials.

2.2.1 Magnetic Soft Materials

Magnetic soft materials are soft materials that respond and move to an external magnetic field. This allows the material to be manipulated by changing the magnitude and the direction of the magnetic field. The way to make these types of soft materials is to embed magnetic materials in the soft material. This is usually done by mixing the magnetic material with the soft material before it is uncured.

The magnetic material that is mixed of the soft material usually comes in the form of particles that are magnetic. These particles can either by microparticles or nanoparticles or both. These particles can also be classified by whether the material is a magnetic hard or soft.

Magnetic soft materials that use soft magnetic materials usually use iron oxides particles embedded in the soft material. Soft materials that use this type of magnetic material will only be magnetic if a magnetic field is nearby. Once the magnetic field is gone or turned off, the magnetization of the particles in the soft materials is also gone. To improve the magnetic properties, some research put the soft material mixed with magnetic nanoparticles in a magnetic field to alignment the particles (Ijaz et al., 2020).

Magnetic hard materials that use hard magnetic materials usually use neodymium nanoparticles embedded in the soft material. Hard magnetic materials can retain their magnetization longer, so this gives rise to different possibilities. Because they retain their magnetization, the soft material can actually be tuned by magnetic field and be programmed to react in a magnetic field in a certain way. While soft magnetic materials may react to both north and south poles the same way, soft materials with hard magnetic materials can respond different depending on the orientation of the magnetic field (Zhao et al., 2019).

8

2.2.2 Application of Magnetic Soft Materials

2.2.2.1 Soft Robotics Soft robots are basically robots made and designed with soft and flexible materials. The efforts to develop these robots have biomimetic roots. Animals, for example, use their soft structured bodies to move in the complex environments. An example of an animal exploiting its soft body is the octopus. The octopus with its soft body can squeeze into tight gaps and blend into the surrounding area to escape predators or to ambush its prey. The soft body of the octopus does not give up strength for flexibility, and it was shown that it can open a jar to get to food. This example and many others have inspired researchers and engineers to develop robots with soft structures. Developing rigid robots to adapt to variable environments would require a lot of work, calculation, and a lot of precision and accuracy (S. Kim et al., 2013).

Three methods have been developed to enhance actuation of soft robots:

- **Dielectric elastomeric actuators (DEAs) made of soft materials that expand and contract through electrostatic forces when a voltage is applied**. DEAs function by using the electrostatic attraction between conductive layers applied to two surfaces of elastomer film. This causes a compressive strain under an electric field. Designs with DEAs require a rigid frame that pre-strains the elastomer. There are a few designs that does not include a rigid frame but they yield very low stress, and they have complex fabrication processes (S. Kim et al., 2013)

- **Shape memory alloys (SMAs with temperature-dependent morphology)**. SMAs deform when cooled but return to its original shape when heated. The force generated by SMAs varies with the temperature change. The challenge is to have a robust way to control temperature in various thermal conditions. Most of the energy consumed is used for heating the SMAs wire which leads to poor efficiency (S. Kim et al., 2013).

- **Application of compressed air or pressurized fluids**. This technique uses compressed air and pressurized fluids. The robot would be deformed by the pressurized air. These actuators show great performance in term of speed

and power density. The challenge with this system is that it is not easy to make a miniaturized version of the system. and an independent source of the air or fluids is needed (S. Kim et al., 2013).

A soft robot was designed using a rubber shell and ferrofluid (Chen et al., 2015). A ferrofluid is a kind of smart material that contains magnetic nanoparticles within a liquid medium. An example of a ferrofluid is a colloidal suspension of magnetite. Because of this suspension, the magnetite assumes the fluidity of a liquid. The fluid can be controlled by the action of a magnetic.

A soft shell will allow that robot to deform and stretch with the fluid inside and allow the robot to adapt in a complex and restricted environment. With this capability of the fluid and the soft exterior, the 'Soft Ball' robot can roll by moving the source of the magnetic field and deform by changing the strength of the magnetic field and can adapt to pass through obstacles as in shown Figure 2.1.

Figure 2.1

Soft Robot Going Through Rectangular Hole Obstacle

Note. Reprinted from Chen, B., Zhu, Y., Zhao, J., & Cai, H. (2015). Design of a prototype of an adaptive soft robot based on ferrofluid. 2015 IEEE International Conference on Robotics and Biomimetics, IEEE-ROBIO 2015, 511–516.
https://doi.org/10.1109/ROBIO.2015.7418819

2.2.2.2 Electromagnetic Micro-actuator A nanocomposite that consist of PDMS and Fe_eO_4 was used as a magnetic material to be utilized in magnetic membrane micro actuators (Paknahad & Tahmasebipour, 2019). Two types of electromagnetic micro-actuators were developed: unidirectional micro-actuator and bidirectional micro-actuator. The nanocomposite was used as an alternative of early electromagnetic actuators that generally use silicon. Actuators with silicon have costly fabrication and have problems with low flexibility and brittleness.

The system consists of the usual electromagnetic membrane micro-actuators, permanent magnet, coil, membrane, and spacer. The operation of the system is as follows: when a voltage goes through the coil terminals, an electrical current goes through the coil and a magnetic field is emitted the coil as shown in Figure 2.2. This magnetic field interacts with the magnetic field from the permanent magnet.

In this paper, a magnetic membrane is used instead of a magnet attached to a membrane as shown in Figure 2.3. The process of make the membrane is shown in Figure 2.4 and 2.5. The spacers that were used in micro-actuator are made of PDMS, which leads to a fabrication process that is simple, a design that is more biocompatible, a greater chance to be applied in drug delivery systems, and more clarity in microfluidic systems.

Figure 2.2

The Schematic Form of the Common Electromagnetic Membrane Micro-actuators
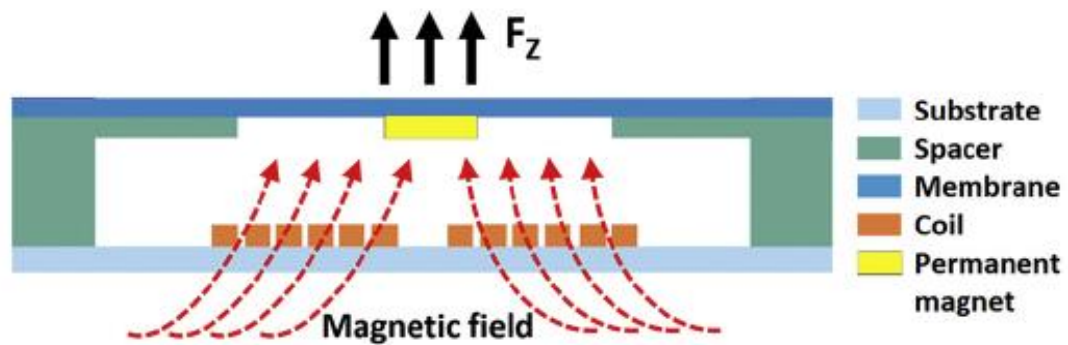
Note. Reprinted from Paknahad, A. A., & Tahmasebipour, M. (2019). An electromagnetic micro-actuator with PDMS-Fe3O4 nanocomposite magnetic membrane. Microelectronic Engineering, 216(March), 111031. https://doi.org/10.1016/j.mee.2019.111031

Figure 2.3

3D Image and Side View of the Proposed Bidirectional Micro-actuator
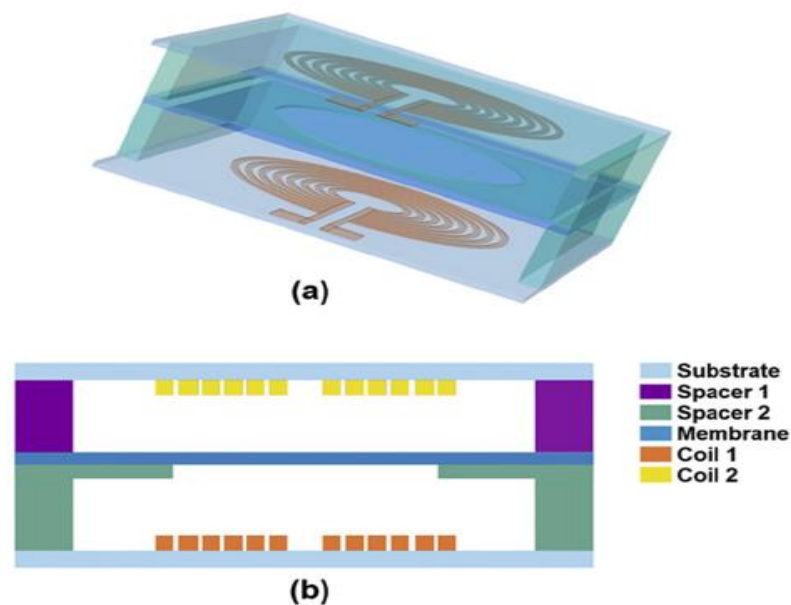
Note. Perspective 3D) image (a) and Side view (b) of the proposed bidirectional micro-actuator. Reprinted from Paknahad, A. A., & Tahmasebipour, M. (2019). An electromagnetic micro-actuator with PDMS-Fe3O4 nanocomposite magnetic membrane. Microelectronic Engineering, 216(March), 111031. https://doi.org/10.1016/j.mee.2019.111031

One of the parameters tested was the effect of the concentration of the nanoparticles to the performance of the actuator is shown in Figure 2.6. Parameter of the concentration (by weight) were 3, 5, 10 15, 20, and 25%. These were tested with two spacers: Spacer 1 with a thickness of 1mm and Spacer 2 with a thickness of 266 µm. In the figure of the results, increasing the Fe_3O_4 nanoparticle concentration to 5% by weight in the membrane increased the membrane displacement. However, increasing the concentration further caused a decrease in displacement due to the membrane have reduced flexibility.

One of the parameters tested was the effect of the concentration of the nanoparticles to the performance of the actuator is shown in Figure 2.6. Parameter of the concentration (by weight) were 3, 5, 10 15, 20, and 25%. These were tested with two spacers: Spacer 1 with a thickness of 1mm and Spacer 2 with a thickness of 266 µm. In the figure of the results, increasing the Fe_3O_4 nanoparticle concentration to 5% by weight in the membrane increased the membrane displacement. However, increasing the concentration further caused a decrease in displacement due to reduced membrane flexibility.

Figure 2.4

Fabrication Process used for Magnetic Nanocomposite
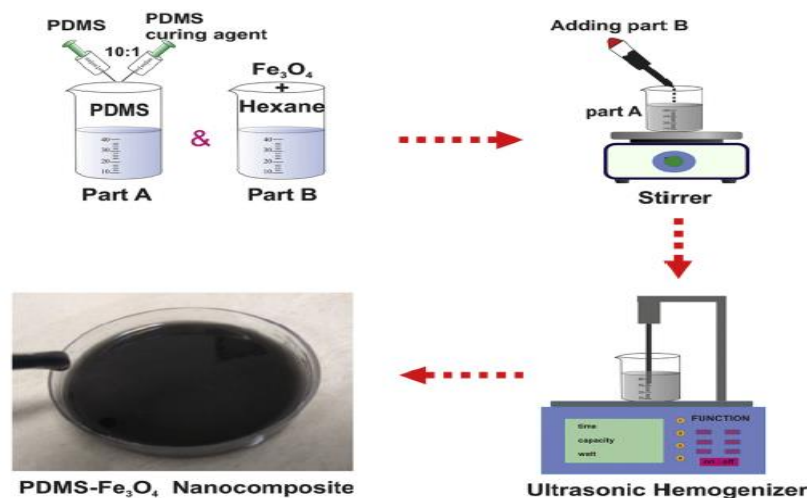
Note. Reprinted from Paknahad, A. A., & Tahmasebipour, M. (2019). An electromagnetic micro-actuator with PDMS-Fe3O4 nanocomposite magnetic membrane. Microelectronic Engineering, 216(March), 111031. https://doi.org/10.1016/j.mee.2019.111031

Figure 2.5

Fabrication Process used for the Magnetic Nanocomposite Membrane
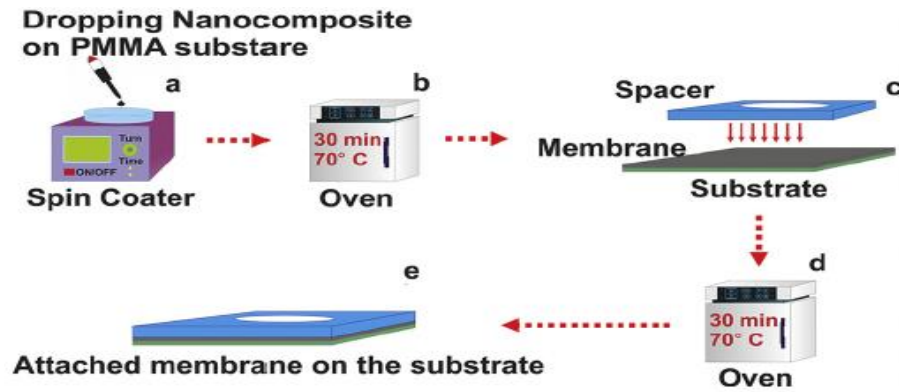
Note. (a) Spin coating, (b) Soft baking, (c) Spin coating, (d) Baking, and (e) Bonding. Reprinted from Paknahad, A. A., & Tahmasebipour, M. (2019). An electromagnetic micro-actuator with PDMS-Fe3O4 nanocomposite magnetic membrane. Microelectronic Engineering, 216(March), 111031. https://doi.org/10.1016/j.mee.2019.111031

Figure 2.6

Effect of Magnetic Nanoparticles Concentration and Spacer Thickness on the Magnetic Membrane Displacement

Note. Spacer 1 and Spacer 2 have thicknesses of 1 mm and 266 μm, respectively. Reprinted from Paknahad, A. A., & Tahmasebipour, M. (2019). An electromagnetic micro-actuator with PDMS-Fe3O4 nanocomposite magnetic membrane. Microelectronic Engineering, 216(March), 111031. https://doi.org/10.1016/j.mee.2019.111031
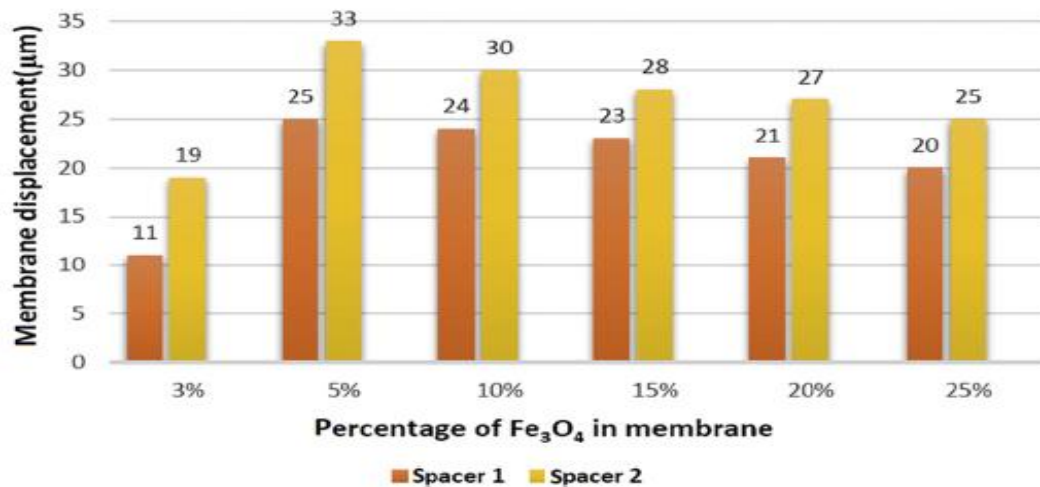
2.2.2.3 Flexible Magnetically Responsive Film The manipulation of droplets is used in many applications, from lab-on-a-chip devices to functional surfaces inspired by nature. There are various techniques of droplet manipulation but position and motion control of pure distinct droplets that is active, fast, precise, and reversible remains elusive. A novel technique uses a permanent magnet and a flexible film that respond to a magnetic field embedded with hierarchical pillars on the surface to manipulation a pure discrete droplet (J. H. Kim et al., 2015). The flexible film with moving hierarchical pillars is fabricated by a solution of uncured polymers and magnetic particles that were self-assembly into pillars under a magnetic field.

The preparation of the film is as follows in Figure 2.7. A solution consisting of magnetic particles and PDMS was prepared by mixing uncured PDMS and hexane that was added with carbonyl iron particles.1.5 ml of the solution was poured into a spray gun and then sprayed onto a substrate made of PDMS that was cured with a neodymium magnet placed underneath. The CI particles and uncured PDMS ordered themselves in the same direction of the magnetic field and formed pillars. The samples then went through thermal curing to fix the pillars that were magnetically aligned, resulting in PDMS and magnetic particles forming into pillar arrays throughout the large area. The micropillar arrays were spray-coated with 0.5% concentration by weight CNPs that was dispersed in 2ml of acetone and then dried for 1 hour at 70°C. This resulted in magnetically responsive cone-like pillar arrays with super hydrophobicity.

A neodymium magnet was placed underneath the films to test the dynamic interaction between the pillar arrays and magnetic field. The changes in the structure were observed with an optical microscope placed above by controlling magnet orientation in the horizontal position. When testing the films, simple and precise control of the array by changing the magnet location was observed.

The film was able to manipulate droplets by moving a magnetic under the film. This works by the pillar arrays near the magnet are bended towards the magnet field that results in a space on the surface as shown in Figure 2.8. The droplet can then be maneuvered towards the desired location along the open space. The direction of the space can be controlled by simply changing the magnet orientation.

Figure 2.7

A Schematic Illustration of the Fabrication Procedure of the Magnetically Responsive
Film
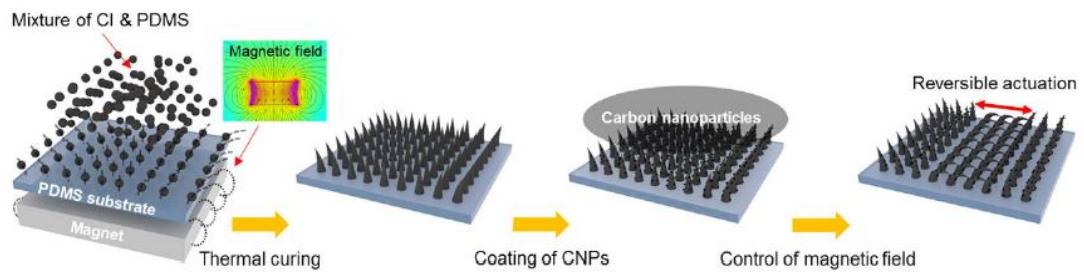
Note. Reprinted from Kim, J. H., Kang, S. M., Lee, B. J., Ko, H., Bae, W. G., Suh, K. Y., Kwak,
M. K., & Jeong, H. E. (2015). Remote Manipulation of Droplets on a Flexible Magnetically
Responsive Film. Scientific Reports, 5, 1–10. https://doi.org/10.1038/srep17843

Figure 2.8

Water Droplet Guided by Magnet Under Film
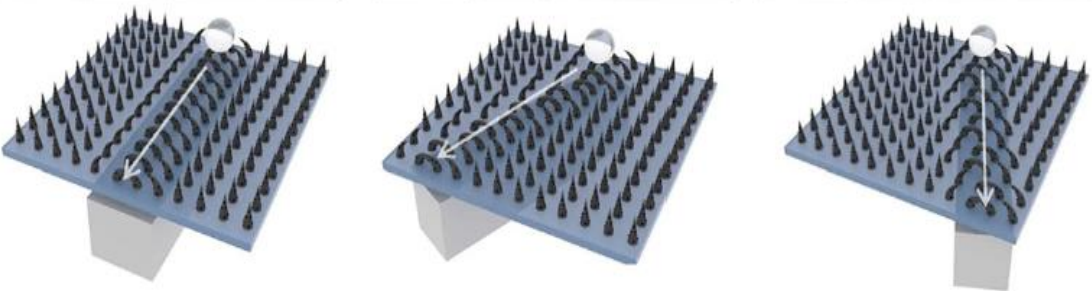
Note. Reprinted from Kim, J. H., Kang, S. M., Lee, B. J., Ko, H., Bae, W. G., Suh, K. Y., Kwak,
M. K., & Jeong, H. E. (2015). Remote Manipulation of Droplets on a Flexible Magnetically
Responsive Film. Scientific Reports, 5, 1–10. https://doi.org/10.1038/srep17843

CHAPTER 3
METHODOLOGY

Methodology is divided into four parts:

- Developing magnetic structure

- Characterization of the structure

- Testing structure integrity of flexible magnetic film

- Investigate angle deflection with respect to different concentrations of nanoparticles and alignment of nanoparticles

Figure 3.1

Process of methodology
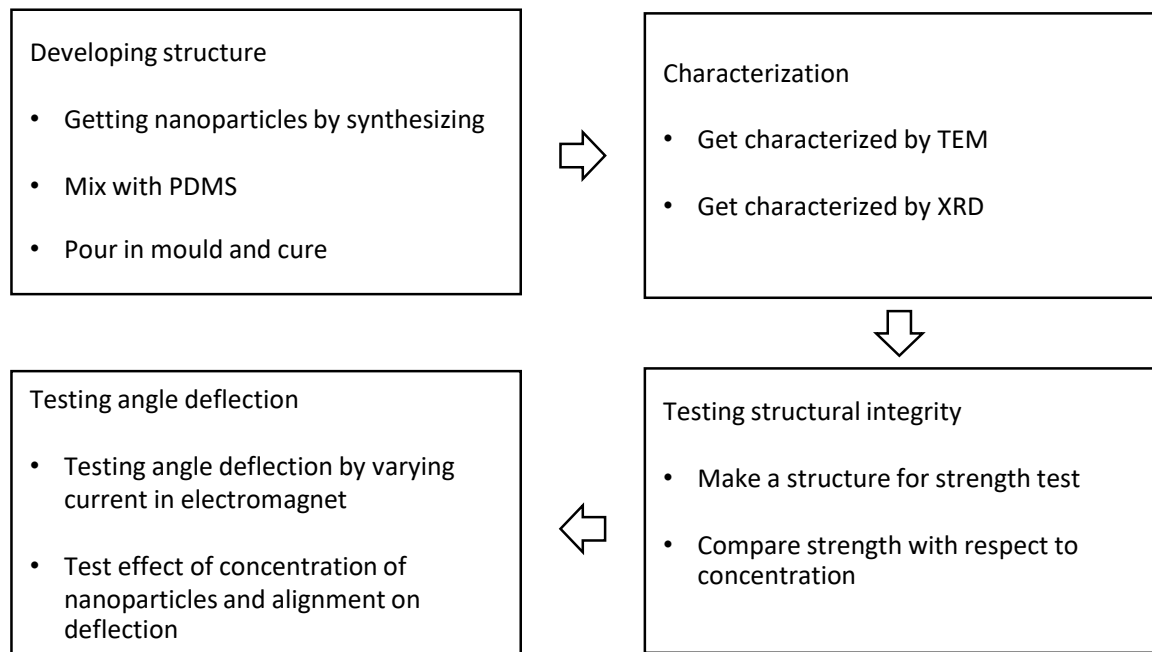
3.1 Developing Magnetic Structure

The project starts by making the magnetic structure. The magnetic structure was made of a polymer called polydimethylsiloxane (PDMS) and magnetic iron oxide (Fe_3O_4) nanoparticles dispersed through the matrix.

3.1.1 Materials

3.1.1.1 Polydimethylsiloxane (PDMS) Polydimethylsiloxane (PDMS) is a material that is classified as a silicone. It can be used for various biomaterial applications, include contact lens. In liquid form, it is colorless, odorless, and has no potential health effects. The material is not considered hazardous, so it is safe for medical use. PDMS is a two-part polymer, which consist of a base elastomer and curing agent. The standard mixing ratio for PDMS is 10-parts base elastomer and 1-part curing agent. This ratio provides the desired mechanical properties and optimum biocompatibility.

3.1.1.2 Magnetic Iron Oxide (Fe_3O_4) Nanoparticles The nanoparticles that are used magnetic iron oxide nanoparticles. There are many iron oxides like Fe_2O_3 or maghemite. In this study, the iron oxide that will be used is Fe_3O_4 which is known as magnetite. The iron oxide nanoparticles behave very different in terms of their magnetic properties. These nanoparticles are also biodegradable, nontoxic, and benign. Because iron oxide nanoparticles are biocompatible, it is used in many biomedical applications and would be an ideal material to use for this study.

To get the nanoparticles, different methods were investigated. One method to synthesis the iron oxide nanoparticles by a chemical process called the co-precipitation method. The co-precipitation is the most common method to synthesis iron oxide and the most straightforward.

The coprecipitation method is a commonly used method due to it being straightforward and relatively easy. This method mainly works by adding a base to a Fe^{2+}/Fe^{3+} salt solution to provide an alkaline environment to generate Fe_3O_4 nanoparticles. The formation of the nanoparticles is formed through nucleation and growth mechanisms. The chemical formation of Fe_3O_4 is shown in the Equation 3.1:

$$Fe^{2+} + 2Fe^{3+} + 8OH^- = Fe_3O_4 + 4H_2O \qquad \text{(Equation. 3.1)}$$
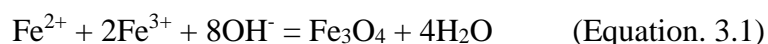
One of the problems when synthesizing iron oxide nanoparticles is that the particles have a strong tendency to agglomerate with each other. Because of this, functionalization of the nanoparticles' surfaces with surfactants are needed to prevent agglomeration. In this study, oleic acid is used for the functionalization of the

nanoparticles based on an articles that studied about the effect of oleic acid on the effect of iron oxide colloidal stability (Lai et al., 2018).

Figure 3.2

Coprecipitation Method
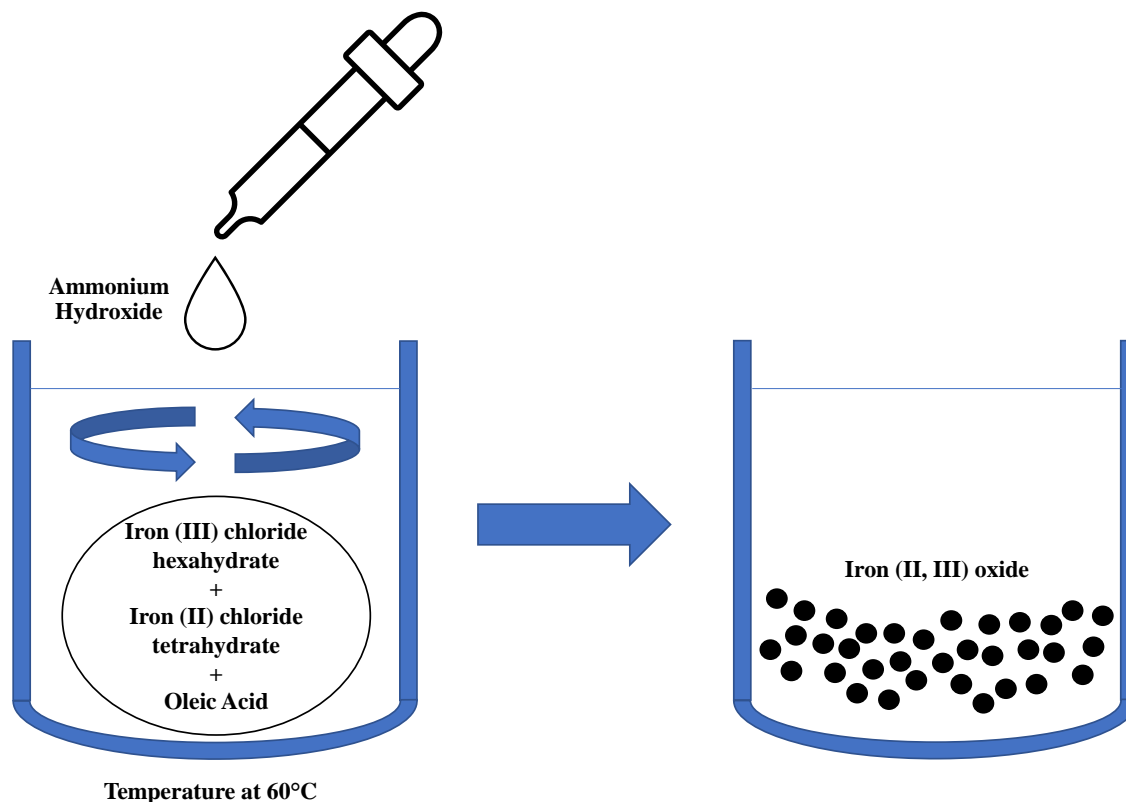
The procedure starts by preparing 100 mL of precursor solution containing 0.030 mol iron (III) chloride hexahydrate, 0.015 mol iron (II) chloride tetrahydrate, and oleic acid that equals 1.5% weight of the aqueous solution. Next, 11.4 mL of ammonium hydroxide (25% ammonia solution) mixed with 100 mL of water is added into the solution that is at 60°C. Mixture will be left under constant agitation until the ammonia solution addition is finished. Magnets will be used to separate nanoparticles. The nanoparticles are then washed with distilled water and ethanol three times.

The nanoparticles are then put in a vacuum oven with silica gel to take out the moisture from the nanoparticles. Taking water from the nanoparticles is a crucial step because PDMS is hydrophobic, so moisture in the nanoparticles will cause the particles to not

be dispersed uniformly in the PDMS. To make sure that all moisture in the nanoparticles are gone, the nanoparticles are baked in the vacuum oven at 70°C for 8 hours. The nanoparticles should come out dry without a sticky texture. Procedure to fabricate the magnetic structure is shown in Figure 3.3.

Figure 3.3

Flow Chart of Fabricating Magnetic Structure
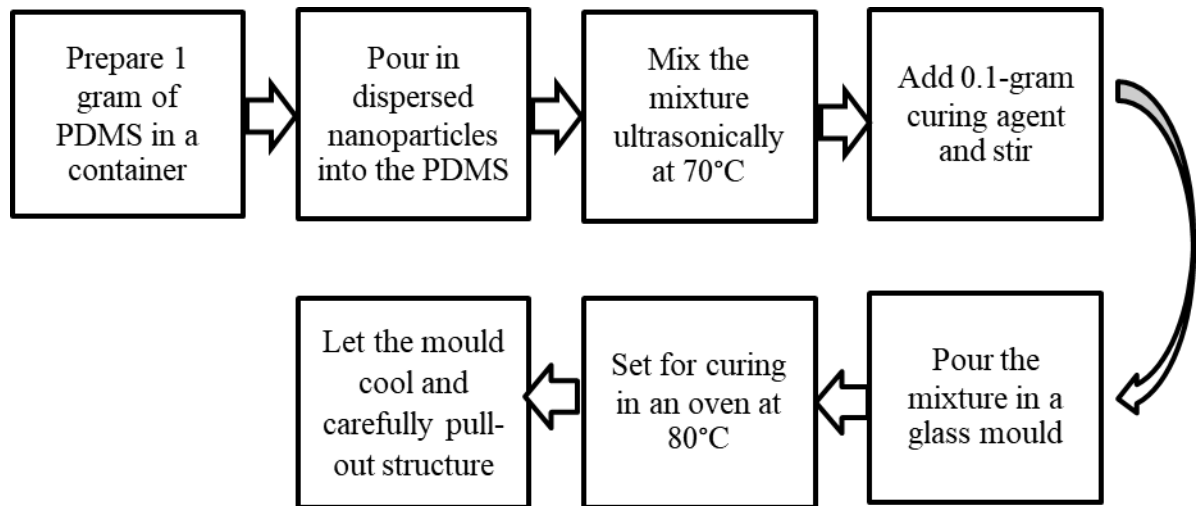
After the nanoparticles are dried, they are dispersed in chloroform by sonication. If 0.2 grams of iron oxide nanoparticle is used, then 1 mL of chloroform should be used. PDMS is then added to the dispersion and then sonicated. The mixture is then sonicated and heated at the same time to evaporate the chloroform.

After the mixing is finished, curing agent is added to the PDMS mixture and then sonicated to ensure the curing agent is uniformly mixed. The mixture is then poured onto a glass mold to make a thin film and then put in the vacuum chamber to be degassed to take out air bubbles in the mixture. The films are then put in the oven at 80°C for 3 hours and then taken out of the mold.

The dimensions of the structure that is aimed for in this project is a thickness of 1 mm, 15 mm wide, and 66 mm long. Multiple structures will also be fabricated with different amounts of nanoparticles to test the effect of the concentration with respect to different parameters such as strength and angle deflection. Some of the structures have the

nanoparticles to be aligned which means that their magnetic domain will point in one direction to make that resultant force stronger when a magnetic field is active. This is achieved by place the uncured structure between two magnets overnight.

3.2 Characterization

3.2.1 Transmitted Electron Microscopy (TEM)

This part of the process will show as the size and the shape of the nanoparticles. The dimension and the shape of the nanoparticles will also be seen through the characterization. A sample of the nanoparticles was sent to the Center of Scientific Equipment for Advanced Research (TUCSEAR) in Thammasat University. The model of the TEM is JEOL, JEM-2100 Plus, JAPAN that uses the software TEM center. The mode that was used for the characterization was TEM and Single Atom Electron Diffraction (SAED). The accelerating voltage that was used is 200 kV.

The sample is a vial of iron oxide nanoparticles dispersed in ethanol and was analyzed using Transmitted Electron Microscope. The solution will be poured over a copper grid and the nanoparticles will attach to the grid. The TEM uses fired electrons that pass through the sample. The preparation is showed in Figure 3.4.

When passing through the sample, the electrons will interact with the sample and their paths will be affected by the interaction. The electrons will then go to a fluorescent screen. How much the path is affected by the interaction correspond to the brightness of the spots of the screen. The images of the sample from the TEM will then be studied and analyzed.

With the TEM, single atom electron diffraction (SAED) was also performed on the sample. When electrons pass from the sample, the electrons scatters in different directions and different angles. The angles and direction that the electron will scatter will depend on the density of the materials and the thickness.

Figure 3.4

TEM Characterization
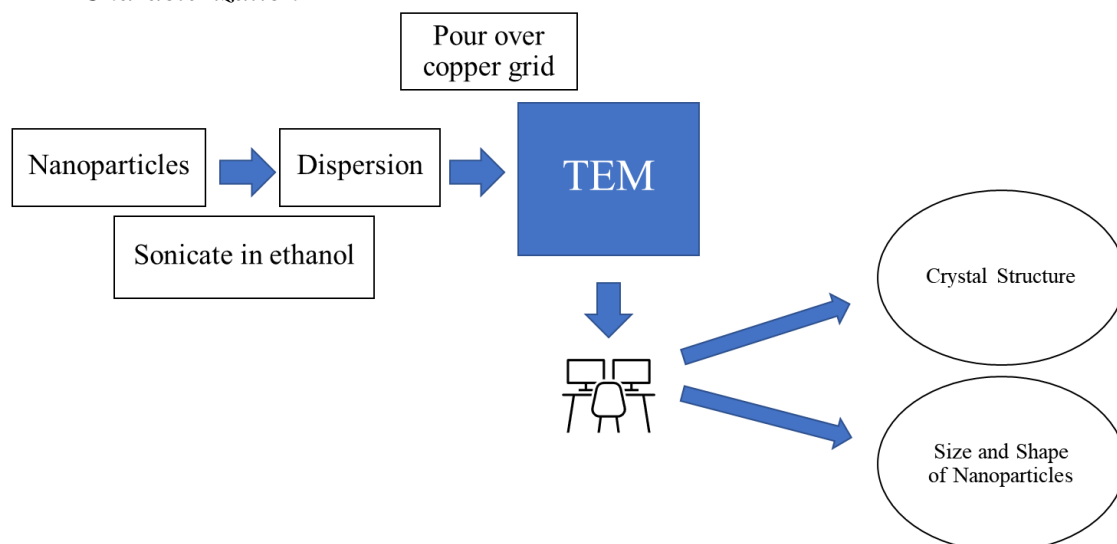
3.2.2 X-ray Powder Diffraction (XRD)

X-ray powder diffraction (XRD) is used to identify the material and the crystallite size of the powder. The characterization with the XRD was performed in the Thailand National Metal and Materials Technology Center (MTEC) in the National Science and Technology Development Agency (NSTDA). The model of the XRD machine is Rigaku, TTRAX III using 18 KW. The XRD machine fires x-rays at the sample in powder that is packed on a dish. The machine will fire the x-rays at different angles. The iron oxide nanoparticles were first synthesized and then dried in a vacuum oven. The nanoparticles were then ground to powder form and placed in a vial. The amount needed from the XRD is approximately 0.5 grams of powder. The powder was then sent to MTEC to be characterized with XRD.

The results of the XRD come in a graph of the intensity with respect to the angle of the x-ray. At certain angles that the graph will show peaks at certain angles called characteristics peaks. These peaks are like the fingerprints of the materials that is unique to the material you are studying. The results can be compared to the standard results that have already been tested from database of XRD results such as The International Center for Diffraction Data (ICDD).

The results can also show the crystallite size of the powder by looking at the biggest peak. The crystallite size is the smallest single crystal of a material in powder form. The crystal structure can be also analyzed XRD. From the characteristic peaks from the graph, the Miller index which is represented by hkl can show the crystal lattices of the material that can give a glimpse of the structure. This can be summarized by Figure 3.5. The crystallite size is found by using Scherr's equation. As mentioned before, the biggest peak in the graph will be studied by using the Scherr's equation. The equation is shown in Equation 3.2.

$$D = \frac{k\lambda}{\beta \cos\theta} \hspace{2cm} \text{(Equation 3.2)}$$

D is the size of the crystallite, k is the shape factor, which is approximated at 0.9, λ is the wavelength of the x-rays, β is the full-width at half maximum, and θ is the Bragg angle.

Figure 3.5

XRD characterization
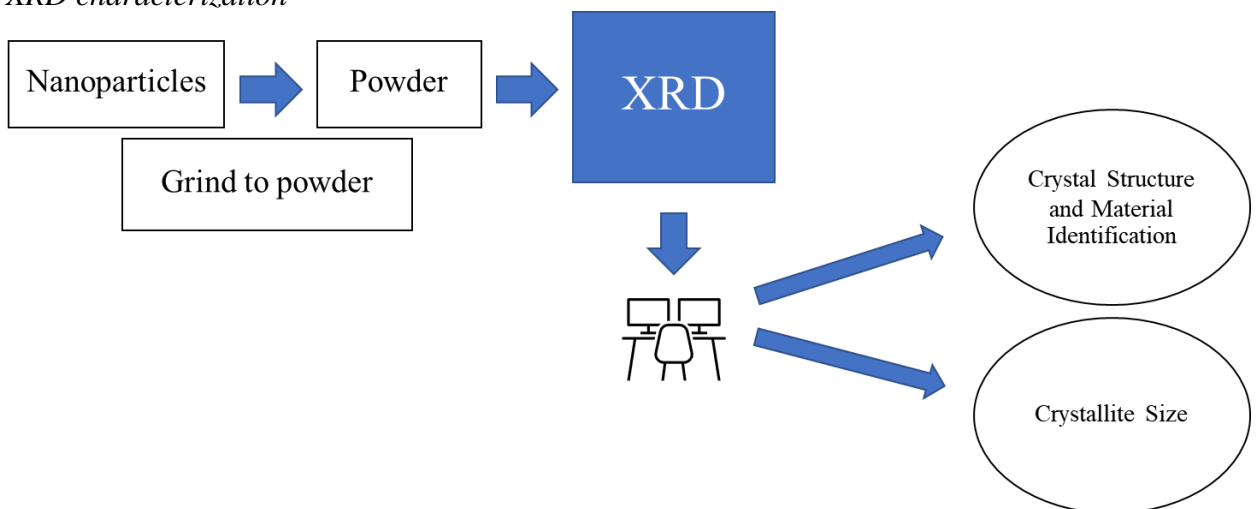
3.2.3 Texture Analysis Test

Once making the structure was completed, the structure integrity was tested. This would be important because it will show how the structure is affected by the nanoparticles and if it is easily broken or not. A different structure of PDMS with the dispersed nanoparticles will be fabricated to suit the testing procedure. A structure with no nanoparticles will also be fabricated to compare the strength of the materials. The

testing procedure will be tested in Characterization and Testing Service Center (NCTC) at NSTDA.

A tensile strength test was conducted using texture analysis test with a texture analyzer Shimadzu EZ-LX. The structure was cramped on the machine and was pulled apart. The machine took measurements of the elongation of the structure and recorded against the applied force. The force measurement was then used to calculate the engineering stress.

Multiple structures with different concentration of iron oxide nanoparticles were fabricated to see the effect of the concentration to the tensile strength of material. The concentrations that were tested for the samples were 0%, 5%, 10%, and 20% by weight of PDMS. The dimensions of the structure that were required for the test are a minimum length of 50 mm, a minimum length of 10 mm, and a thickness of 1mm. Each concentration has three samples to have an average.

Figure 3.6

Tensile Stress Testing Procedure
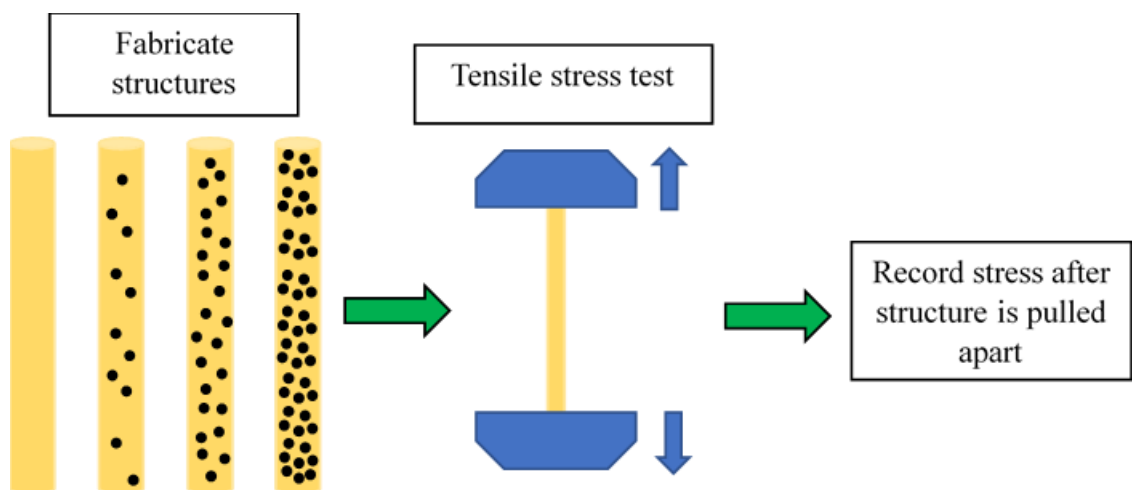
3.3 Investigating Movement of Structure

The structure was made as the long piece of the magnetic film. The magnetic film that was made was divided into six pieces to have a sample size of at least five. The

approximate dimensions of each piece are 33 mm in length, 5 mm in width, and 1 mm in thickness. The structure is then attached to an acrylic piece with only 10 mm of its length sticky out.

The small thin magnetic film was placed in a vertical position with an external magnetic field source as shown in Figure 3.7 that was placed approximately 5 mm from the magnetic film. To control the movement of the structure, an electromagnet was used. The electromagnet was switched on to make the structure move and the magnetic field can be varied by changing the current going through the electromagnet. In this stage, the movement was investigated and show how that structure behaves in a magnetic field from an external source.

The structure was tested by varying different concentration of nanoparticles and alignment of the magnetic domain of the nanoparticles. The effect of concentration on the movement of the structure was tested to see how much it will impact the movement and control of the structure. The alignment of the magnetic domains was also be tested to see if there is any effect of the deflection.

Figure 3.7
Experimental Setup
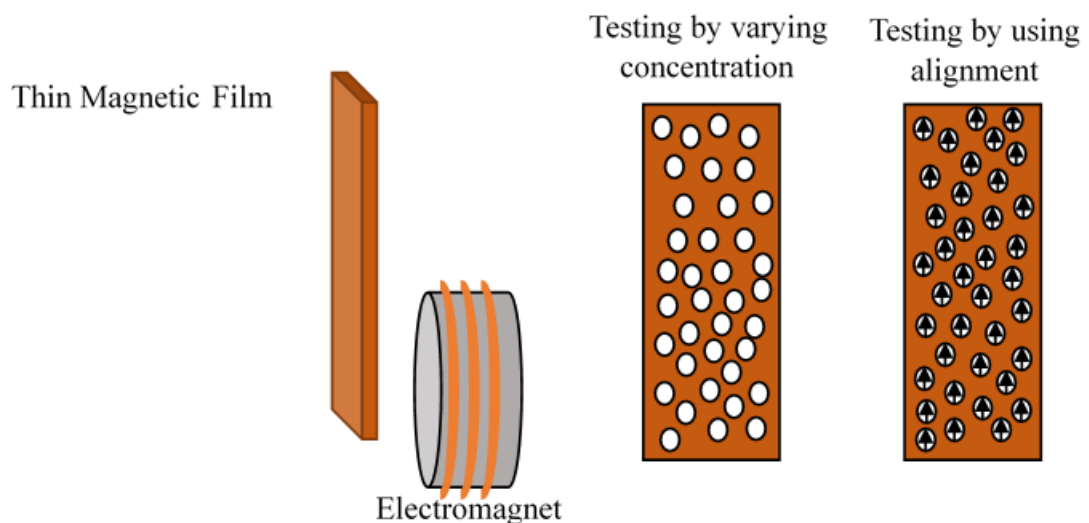
While varying the current in the electromagnet, pictures were taken of each position of the magnetic structure. The angle deflection will then be measured by using a software called ImageJ. The angle deflection will be then saved and analyzed and compared with respect to concentration of the nanoparticles and the alignment of the nanoparticles. Using the data gathered, the sensitivity of the magnetic film will then be calculated.

The electromagnet that was used is XP34/25 and uses up to 12 Volts. It is advertised to be able to lift 20 kg. The dimensions are 34 mm in diameter and 24 mm in length with a weight of 150 grams. To approximate the magnetic field with the corresponding current, the current must be found that corresponds to the amount of force that was advertised.

Though there were not specifications about the current of XP 34/25, there is another electromagnet model that has similar specifications. The MK-P34/25 model has the same specifications in terms of the voltage, the holding force, and the dimensions. According to its specifications, the current that is recommended to be used with the electromagnet is 0.5A. With this information, we can approximate the number of coils in the electromagnet.

To find the number of coils in the electromagnet, the magnetic field needs to be calculated with the corresponding holding force which 20 kg or 196.2 N. Equation 3.3 is an equation that is used to find the effective lifting force and can be used to solve for the magnetic field (Engineers Edge, n.d.).

$$F = \frac{B_m^2 \, A_m}{8\pi \times 10^{-7}} \qquad \text{(Equation 3.3)}$$

F is the force in Newtons, B_m is the magnetic flux per unit area which is in Tesla, and A_m is the area if the magnet contacting the steel plate. From the dimensions and specifications, it is calculated that the magnetic field is 0.737 T. Next, this value will be used to find the number of coils with Equation 3.4.

$$B = \mu_0 \frac{NI}{l} \qquad \text{(Equation 3.4)}$$

B is the magnetic flux density of the solenoid, μ_0 is the magnetic constant that is equal to 1.26 x 10^{-6}, l is the length of the solenoid, and N is the number of coils. From the values that was precisely calculated with the values that was given, the number of coils is equal to 29246 turns. With the value of the number of turns calculated, the magnetic field corresponding to the current supplied can be calculated. The magnetic field and the current that will be varied is shown in Table 3.1.

Table 3.1

Current with Corresponding Magnetic Field

Current (A)	Magnetic Field (Tesla)
0	0
0.070	0.1
0.14	0.2
0.20	0.3
0.27	0.4
0.34	0.5
0.41	0.6
0.47	0.7
0.54	0.8
0.61	0.9
0.68	1

The first step was to compare the initial position of the structure which occurs at 0 Tesla to the positions of the structures at other magnitudes of the magnetic field. The results were then plotted on the graphs to compare the results of different concentrations and alignment. The structure's concentration of iron oxide nanoparticles that was tested was 0%, 5%, 10%, and 20% by weight of PDMS.

From the plotted results, the graphs underwent curve fitting to find the linear equation of the relationship between angle deflection and magnetic field. From the equations,

the slope of the linear equation will be used to find the sensitivity which is defined in this study as the ratio of angle deflection and magnetic field.

3.4 Initial Testing

Before doing the experiment, there were some initial tests that were done. One test involved the alignment of the magnetic domain of the nanoparticles and another test involved testing the deflection with magnets.

3.4.1 Aligning Magnetic Domains

The first step of this initial test is to have a small piece of magnetic structure. The magnetic structure was made using glass mould with the PDMS and nanoparticle mixture poured in it. The structure was then baked in the oven at 80°C for 3 hours. There four samples that were made with the conditions 10% concentration that were aligned and not aligned, and 20% concentration that were aligned and not aligned.

The alignment was achieved by placing the sample between two magnets and leaving it overnight to partially cure. The sample was then put in the oven to completely cure. The samples were then taped at the end of stripes of paper and then made to hang vertically as shown in Figure 3.8. The samples were then tested by moving a N35 neodymium magnet slowly towards them to see when samples would react first.

Figure 3.8

Alignment Test Setup

3.4.2 Deflection with magnets

This initial test was setup to demonstrate the effect of concentration and angle deflection as shown in Figure 3.9. The magnets that were used in this setup were N45 neodymium magnets that were 30 mm in length, 20 mm in width, and 5 mm in thickness. To vary the magnetic field, the number of magnets were increased to increase the magnetic field strength. The 15 mm wide thin film was attached to an acrylic board with approximately 17 mm sticking out. Because of the initial curve of the thin films, the first magnet was used to straighten up the film. The angle deflections were then measured and compared with the other concentrations.

Figure 3.9

Deflection Initial Test Setup
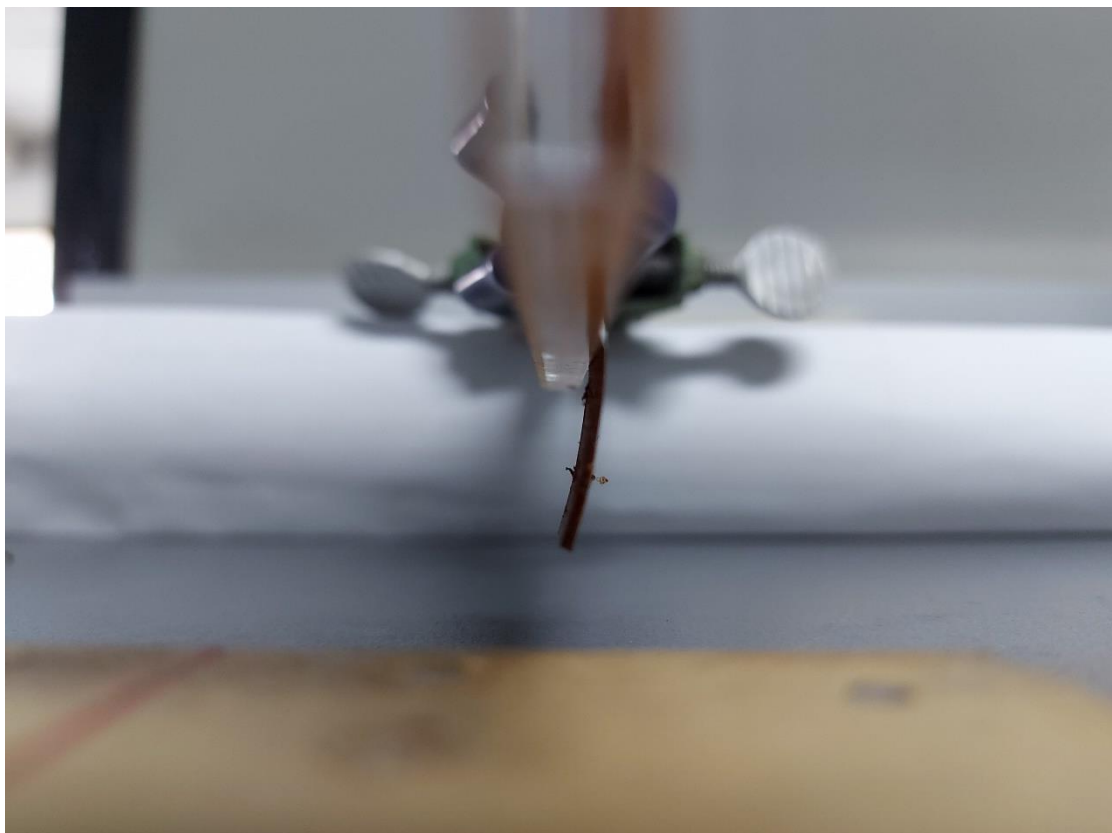
CHAPTER 4

RESULTS AND DISCUSSION

4.1 Iron Oxide Nanoparticle Characterization

Characterization was mainly performed on the iron oxide nanoparticles. Transmitted Electron Microscope (TEM) was used for image the nanoparticles. X-ray Powder Diffraction (XRD) was also used to estimate the crystallite size and indexing the crystal planes. Texture Analysis Test was performed to evaluate the tensile strength of the nanocomposite at different concentrations.

4.1.1 Transmitted Electron Microscope (TEM) Images and Results

The characterization of the TEM was performed in the Center of Scientific Equipment for Advanced Research (TUCSEAR) in Thammasat University. The images of the TEM are shown in Figure 4.1.

Figure 4.1

TEM Images of Iron Oxide Nanoparticles
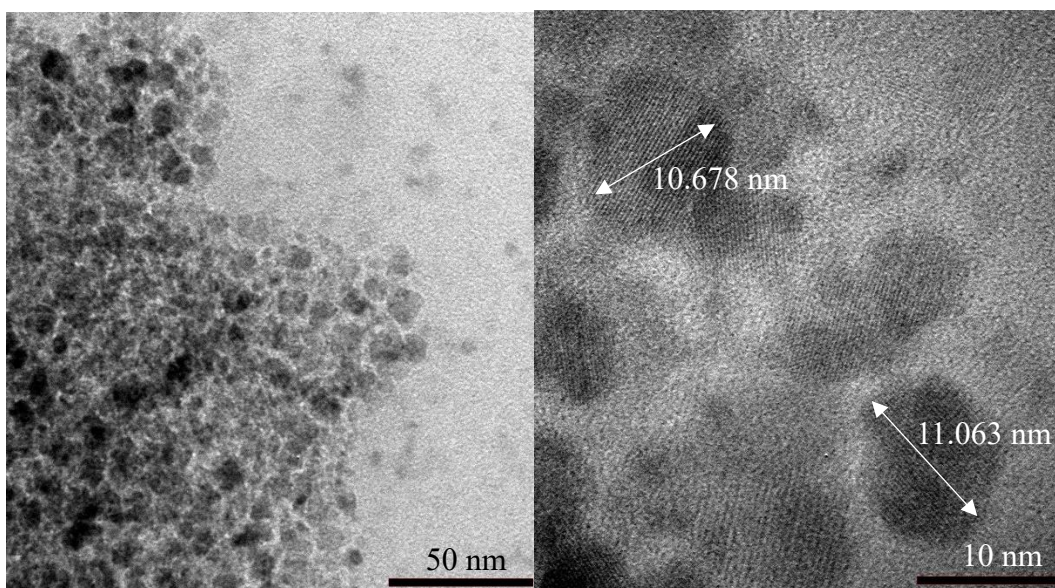
From Figure 4.1, the nanoparticles are in very close contact with each other and also overlapping with each other so using imaging software would be very difficult to use in this case to find the average size. There were some that were able to measure the size and the approximate average is around 10 nm.

With the TEM, single atom electron diffraction (SAED) was also performed on the sample. When electrons pass from the sample, the electrons scatters in different directions and different angles. The angles and direction that the electron will scatter will depend on the density of the materials and the thickness. The result will be an image of a diffraction pattern to show the crystal structure of the material, which is shown in Figure 4.1.

In Figure 4.2, it is shown that the diffraction pattern is a made of rings called continuous Debye rings. This pattern occurs when there are a large number of randomly oriented grains in the material. This is because SAED was performed on a group of particles instead of a single particle. Because of the particles being in very close proximity with each other and also overlapping, doing SAED on a single particle is not possible.

Figure 4.2

SAED of Iron Oxide Nanoparticles
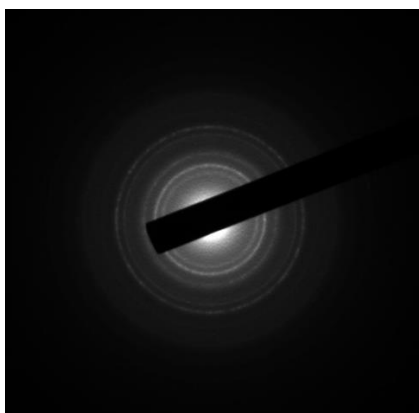
Although the SAED results was not what intended, the Debye rings can still be measured to find the spacing between the crystal planes of the nanoparticles. This is done by using ImageJ by measuring the brightest rings in Figure 4.7. The brightest of

these rings shows that the crystal structure with this spacing is the most predominant in all the nanoparticles. The spacing is the reciprocal of the radius of the Debye rings.

Table 4.1

Spacing of the Crystal Plane Calculated from Debye Rings

Diameter (1/nm)	Radius (1/nm)	d Spacing (nm)
6.374	3.187	0.3138
7.857	3.929	0.2546
9.451	4.726	0.2116
12.692	6.346	0.1576
13.187	6.594	0.1517

From Figure 4.7, the second ring with the diameter is the brightest of all the rings. This ring has the diameter of 7.857 nm^{-1} and calculating the d spacing from this value yields 0.2556 nm. To confirm this, X-ray powder diffraction be used and compared with these values in Table 4.1.

From the pictures that were taken from the TEM, the crystal planes can be seen in the nanoparticles due to the TEM being HRTEM. The crystal planes seen in Figure 4.3 all have a single crystal grain and a single crystal orientation. To analyze the crystal spacing of the nanoparticles, Fast Fourier Transform was used with the software ImageJ that is shown in Figure 4.4. This changes the image from the HRTEM to be an image with a diffraction pattern which can be used to find the spacing of the crystal planes.

Figure 4.3

Crystal Plane of Iron Oxide Nanoparticles
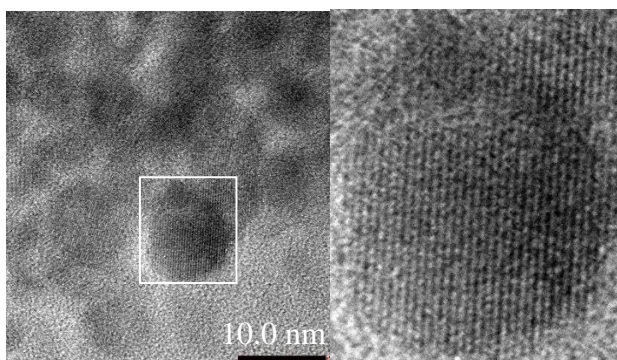
From Figure 4.4, the pattern is a diffraction pattern that consist of three dots. These three dots occur when the crystal planes go along a single direction. Using ImageJ, the spacing of the crystal plane was calculated from the diffraction pattern. Analyzing the diffraction pattern of the image using FFT, the spacing between the crystal plane is approximately 0.26 nm. Measuring multiple nanoparticles, there were values that came up from FFT such as 0.31 nm, 0.15 nm, and 0.21 nm but the spacing that comes up the most is 0.26 nm, which matches with the result from the brightest Debye ring from the SAED.

Figure 4.4

Fast Fourier Transform of Crystal Plane
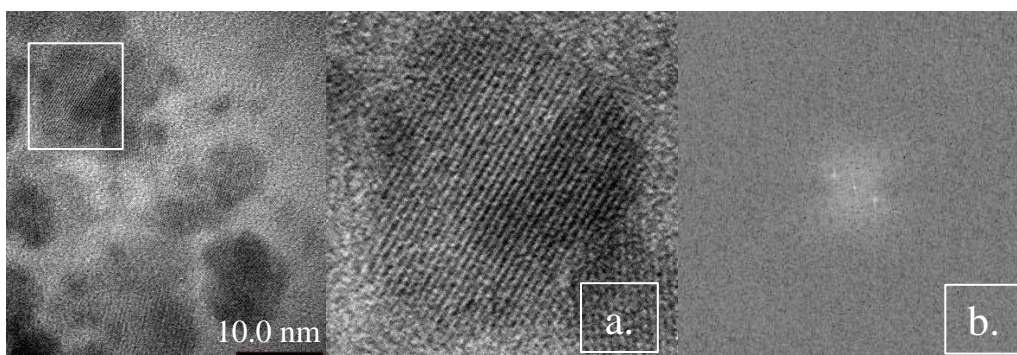
Note. a) Area that FFT was used, b) Diffraction pattern from FFT

4.1.2 X-ray Powder Diffraction (XRD) Results

The characterization with the XRD was performed in the Thailand National Metal and Materials Technology Center (MTEC) in the National Science and Technology Development Agency (NSTDA). The model of the XRD machine is Rigaku, TTRAX III using 18 KW.

The powder was first packed on a dish and then placed in the XRD machine. The machine will fire X-rays that have a wavelength of 0.159 nm at different angles from $2\theta = 5°$ to $2\theta = 80°$. The results will be a graph of intensity with respect to the angle. In the graphs, the peaks can show crystallize size and the crystal structure. The results are shown in Figure 4.5.

Figure 4.5

Graph of XRD of Iron Oxide Nanoparticles
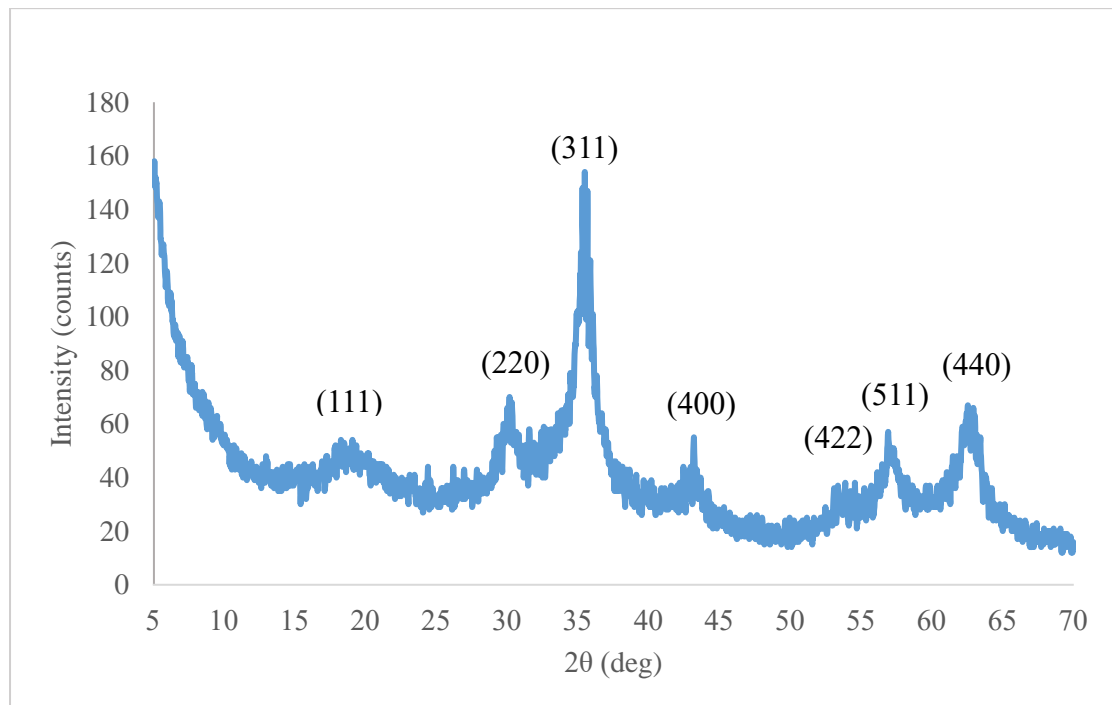
In the graph from Figure 4.5, there are six characteristic peaks. The peaks occur at $2\theta = 18.50°$, $30.36°$, $35.50°$, $43.22°$, $56.92°$, and $62.96°$. The angles are consistent with the corresponding planes (111), (220), (311), (400), (422), (511), and (440) that were

calculated using Bragg's Law which is shown in Equation 4.1. The peaks show that powder is a match of magnetite or Fe_3O_4 from JCPDS card No. 19-0629.

$$n\lambda = 2dsin\,\theta \qquad \text{(Equation 4.1)}$$

With the values of 2θ from the peaks from the graph, we can find the spacing d with these values by using Bragg's Law. In Bragg's Law, λ is the wavelength of the x-rays which is 0.159 nm, θ is the angle of the x-ray at which it was fired, and n is an integer. The values of the d from each angles are shown in Table 4.2.

Table 4.2

Spacing between Crystal Planes Calculated from Bragg's Law

2θ (deg)	θ (deg)	d (nm)	hkl
18.5	9.25	0.495	111
30.4	15.2	0.304	220
35.5	17.8	0.261	311
43.2	21.6	0.216	400
53.9	27.0	0.175	422
56.9	28.5	0.167	511
63.0	31.5	0.152	440

From the Figure 4.5, the value of 2θ that has the highest peak is 35.5° which has a d spacing of 0.261 nm. This corresponds well with the results of SAED from HRTERM that shows that brightest Debye ring to have the d value of 0.255 nm. There are also other values from SAED that matches with the results of XRD, as shown in Table 4.3.

Table 4.3

Comparison of XRD and SAED Results of Spacing

d from XRD (nm)	d from SAED (nm)	Difference (%)
0.304	0.314	-3.35
0.261	0.255	2.39
0.216	0.212	1.97
0.167	0.158	5.54
0.152	0.152	0.378

Other values such as d = 0.175 nm and d = 0.495 nm were not observed in the SAED results since there may not be as many nanoparticles that have these crystal structures to have bright Debye rings. This can also be seen in the XRD graph in Figure 4.10 that shows when 2θ = 18.5° and 53.9°. The peaks of these angles in the graph are not as high as the other angles. From these results from two sources, the iron oxide nanoparticles mostly have crystal structures with Miller's Index of (220), (311), (400), (511), and (440).

From the largest peak in the graph, the crystallite size can also be calculated using Scherr's equation which is shown in Equation 4.2. From Scherr's equation, crystallite size is calculated to be 11.8 nm.

$$D = \frac{k\lambda}{\beta \cos\theta}$$ (Equation 4.2)

D is the size of the crystallite, k is the shape factor which is approximated at 0.9, λ is the wavelength of the x-rays, β is the full-width at half maximum, and θ is the Bragg angle.

Comparing the crystallite size with the size that was measured from the HRTEM images, the values are quite close to each other. Because of this, the crystal structure of the nanoparticles can be concluded to be a single grain in each nanoparticle. This can

also be supported by the images of TEM such as in Figure 4.3 as the grain does in one direction.

4.1.3 Texture Analysis Test

The texture analysis test is a test to evaluate the tensile strength the nanocomposite at four concentrations of iron nanoparticles in the nanocomposite by weight. The concentrations are 0%, 5%, 10%, and 20%. The samples are in the form of a film that is 1 mm thick, 15 mm wide and 66 mm long. The samples were prepared using the synthesized iron nanoparticles mixed with PDMS. The samples were then baked at a temperature of 80°C for three hours except for the samples with 20% concentration which bakes for 5 hours.

The results of each concentration are from the average of three samples for each concentration. The results are in the form of graphs that compares the force when the samples break with the concentration of nanoparticles and the Young's Modulus with the concentration. The results of both are shown in Figures 4.11 and Table 4.4.

From the results in Figure 4.6 and Table 4.4, the sample with 0% concentration or just plain PDMS has the highest value in terms of both force and Young's Modulus while the other values show lower values of both. This is to be expected because adding nanoparticles to any nanocomposite will affect the properties of the composite negative after a certain point. This can be confirmed in an article about an electromagnetic actuator that also uses a PDMS and iron oxide nanocomposite (Paknahad & Tahmasebipour, 2019).

From Figures 4.6 and Table 4.4, it can be seen that as the concentration increases to 5% and 10%, the force and the Young's Modulus decreases, but the values of both force and Young's Modulus increases again at 20% concentration that is most likely caused by the curing time in the oven. The 5% and 10% concentration samples were baked at 80°C for 3 hours while the 20% concentration samples were baked for 5 hours. This curing time difference was necessary to completely cure the 20% concentration samples as only baking for 3 hours resulted in the sample being not completely cured and impossible to take out of the mould. This was not studied in detail and will need to be investigated in the future.

Table 4.4

Young's Modulus of Nanocomposites at Each Concentration

Concentration	Averaged Young's Modulus (MPa)	Standard Deviation
0%	0.91442	0.13531
5%	0.36496	0.06103
10%	0.19835	0.02637
20%	0.26449	0.11244

Figure 4.6

Breaking Force of Film with respect to Concentration of Iron Oxide Nanoparticles
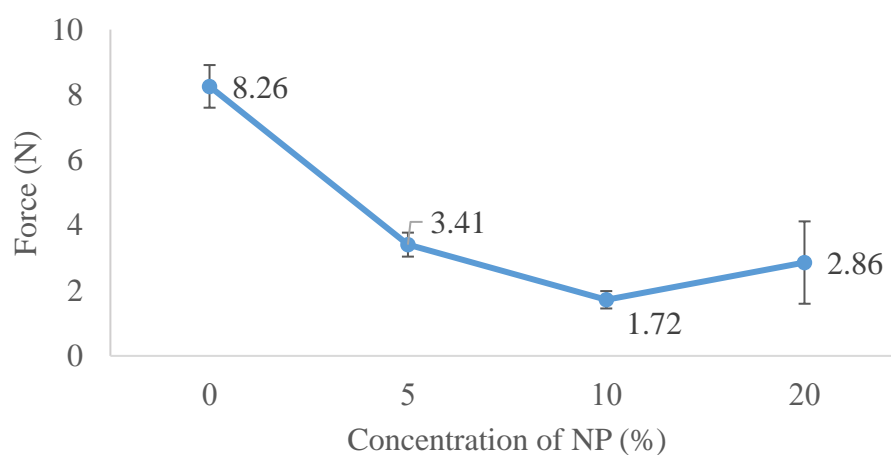
Figures 4.7, 4.8, 4.9, and 4.10 shows that stress-strain curve of the nanocomposites samples. The curves of the three samples were plotted on the graph and then averaged. The samples of 5% and 10% concentration showed less variation than curves of the 0% and 20% concentration samples. This shows that there must have been factors that affect the strength of the samples such as amount of curing agent or baking time.

Figure 4.7

Stress Strain Curve of Plain PDMS
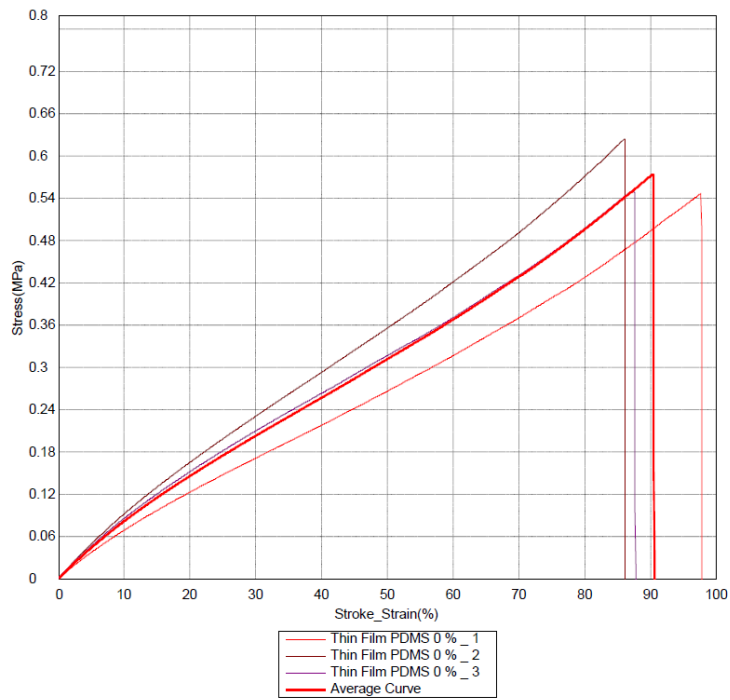
Figure 4.8

Stress Strain Curve of 5% PDMS Nanocomposite
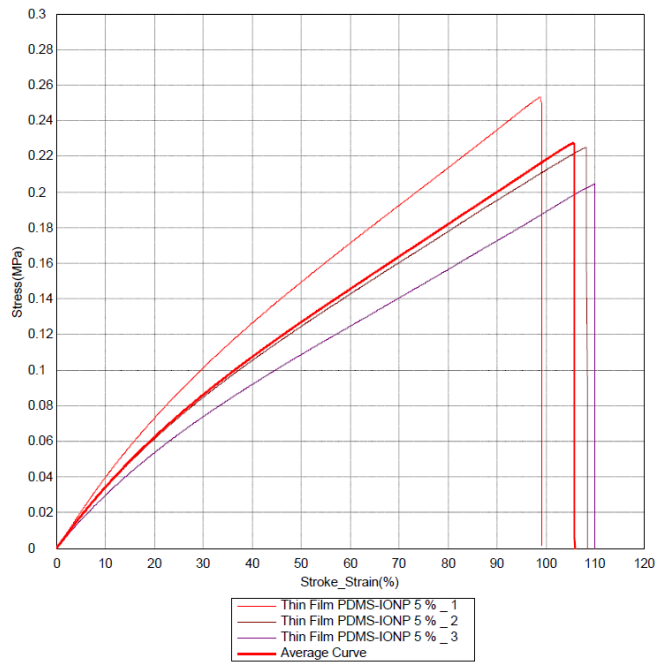
Figure 4.9

Stress Strain Curve of 10% PDMS Nanocomposite
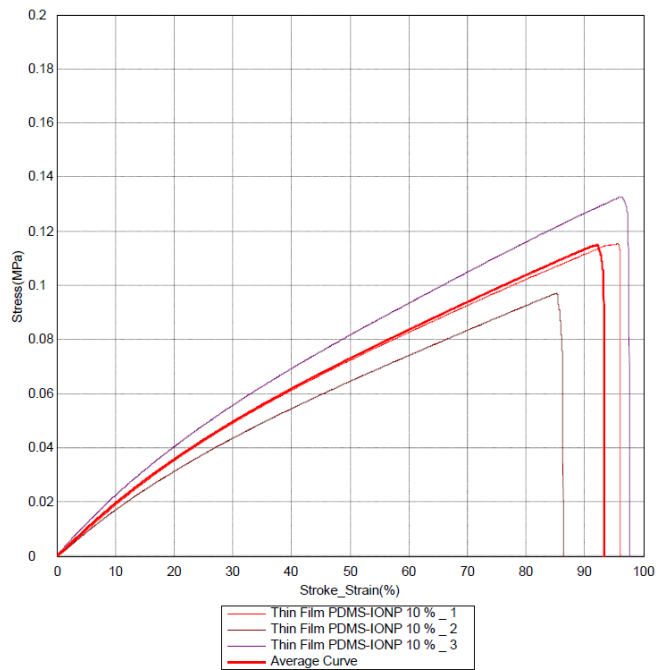
Figure 4.10

Stress Strain Curve of 20% PDMS Nanocomposite
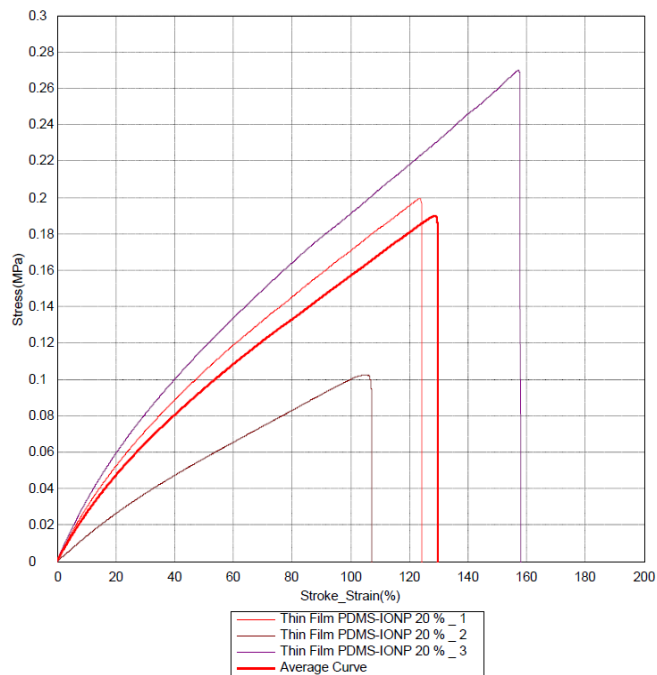
4.2 Deflection of the Magnetic PDMS Film under Applied Magnetic Field

4.2.1 Initial Testing

From this initial test, it is shown the alignment of the magnetic domains of the nanoparticles influences the magnetic behavior of the structure and can be achieve in a simple setup that consist of two magnets.

Figure 4.11

10% and 20% Concentration Alignment Test
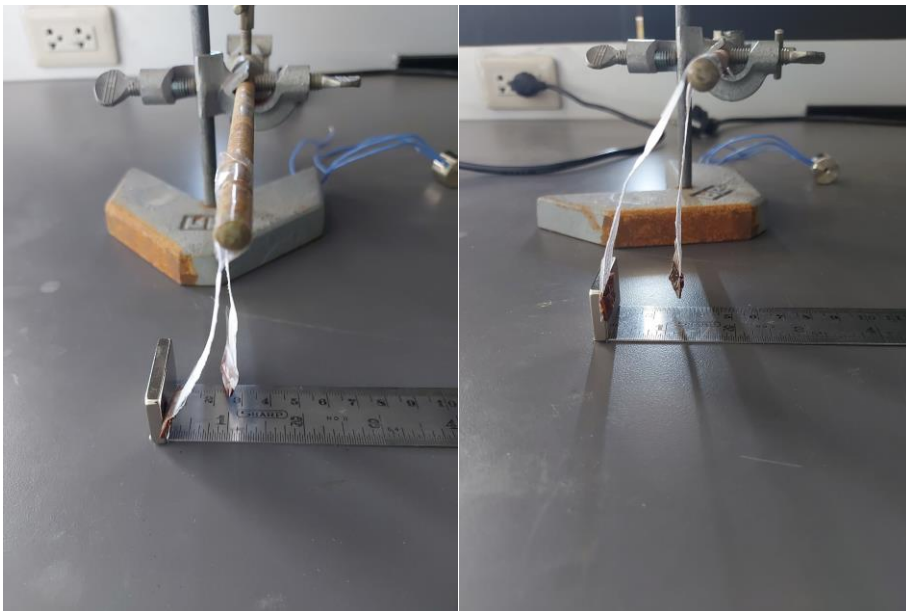
Note. The 10% concentration sample is on the left while the 20% concentration sample is on the right.

From Figures 4.11, the samples are tested using a magnet attached to a ruler to measure when the samples get attracted the magnet. Figure 4.11 shows that samples with 10% concentration and with 20% concentrations. In both cases, the aligned samples seem to have reacted first to the magnet. To test this further, the magnet was moved back and forth and samples that were aligned reacted while the non-aligned samples did not.

The concentrations that were tested were 5%, 10%, and 20% by weight which are shown in Figure 4.12, Figure 4.13, and Figure 4.14.

Figure 4.12

5% Concentration Angle Deflection
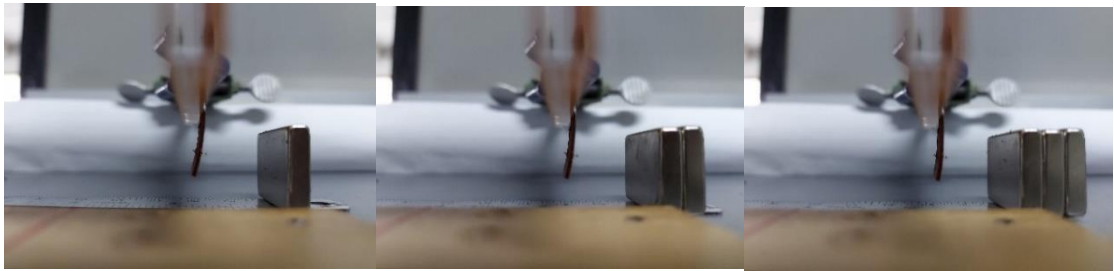
Figure 4.13

10% Concentration Angle Deflection
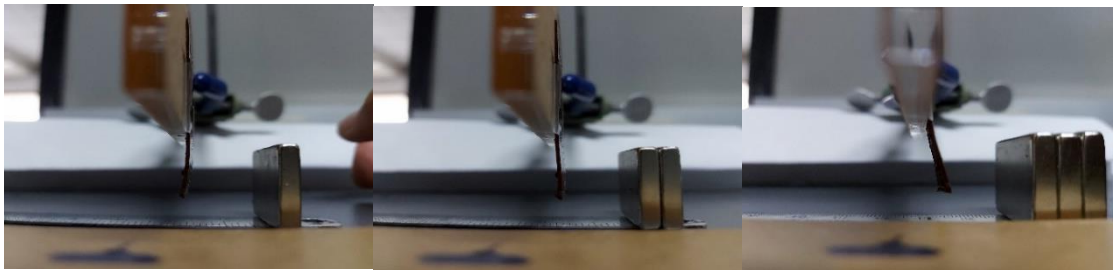
Figure 4.14

20% Concentration Angle Deflection
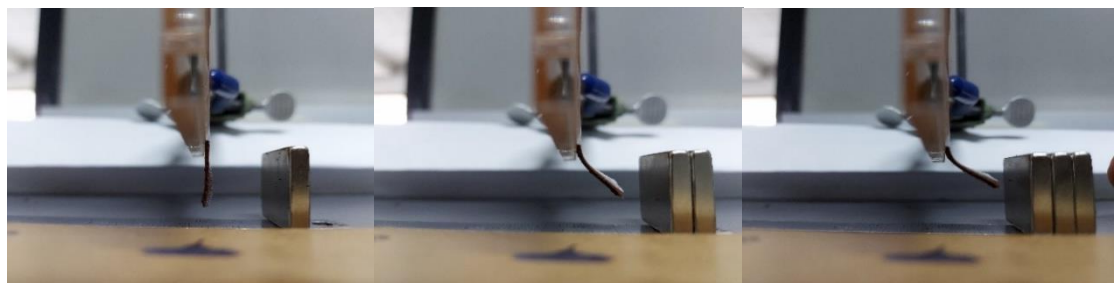
Figure 4.15

Angle Deflection of Initial Test
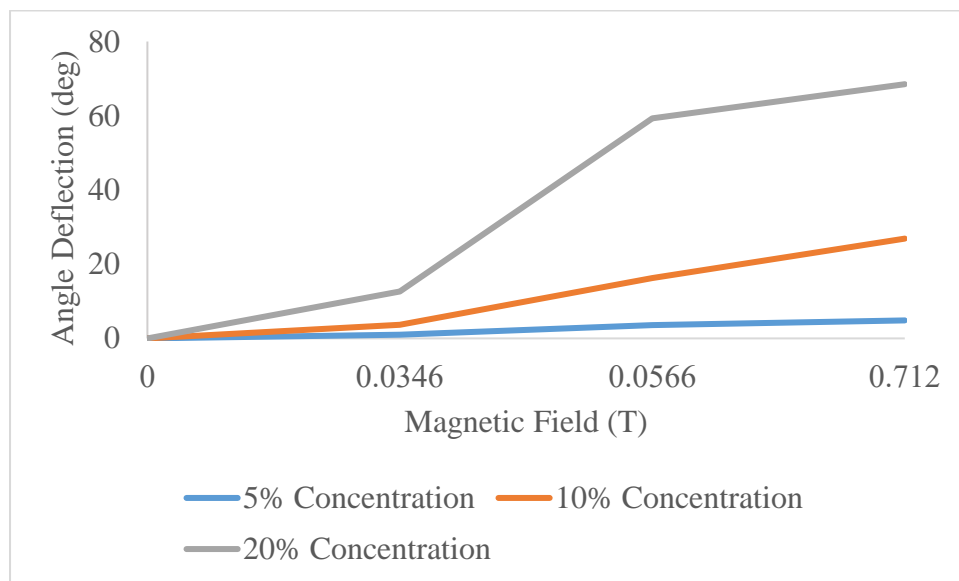
From Figures 4.15, it can be seen that there is that increasing the concentration increase the angle deflection of the structure. The value of the magnetic field comes from the magnetic field from 1 to 3 N45 neodymium magnets that have the dimension of 30 mm in length, 20 mm in width, and 5mm in thickness. The result from this test has some clear different in the angle deflection but the data points are very few. Therefore, electromagnets will be used for the experiment and get more data points. The problem with electromagnets is that the magnetic field tends to be negligible at a distance, so the structure must be at a closer distance to the electromagnet compared to the neodymium magnets.

4.2.2 Angle Deflection

The results are from the experimental setup that consist of a magnetic film placed in front at approximately 5 mm from an electromagnet as shown in Figure 4.16. The current was varied to change the magnetic field of the electromagnet and the magnetic structure position was taken by a camera. The conditions involved the concentrations of the structure and the alignment of the nanoparticles. Overall, there were seven conditions of the structure with each condition having five samples.

Figure 4.16

Angle Deflection of Magnetic Film at 0 and 1 Tesla from Left to Right
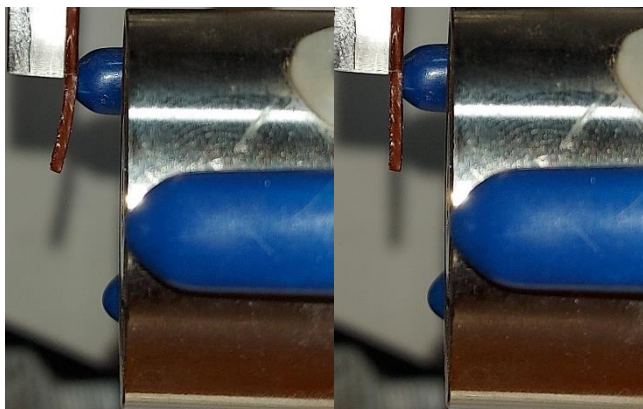
Note. The magnetic field was varied by varying the current going through the electromagnetic. The angle deflection with respect to the current can be referred to Table A19 to Table A24 in the Appendix.

Figures 4.17 and 4.18 shows the comparison of the angle deflection and the concentration of the samples of iron oxide nanoparticles from the averages from 5 samples from each concentration. Figure 4.17 shows the angle deflection with respect to the magnetic field of the non-aligned samples and Figure 4.18 shows the angle deflection with respect to the magnetic field of the aligned samples. Both figures show that increasing amount of the iron oxide nanoparticles can increase the angle deflection of the structure, whether it is aligned or not. In both figures, increasing the concentration to 20% also increased the final angle deflection by around 300%.

Figure 4.17

Angle Deflection of Non-aligned Samples with respect to Magnetic Field
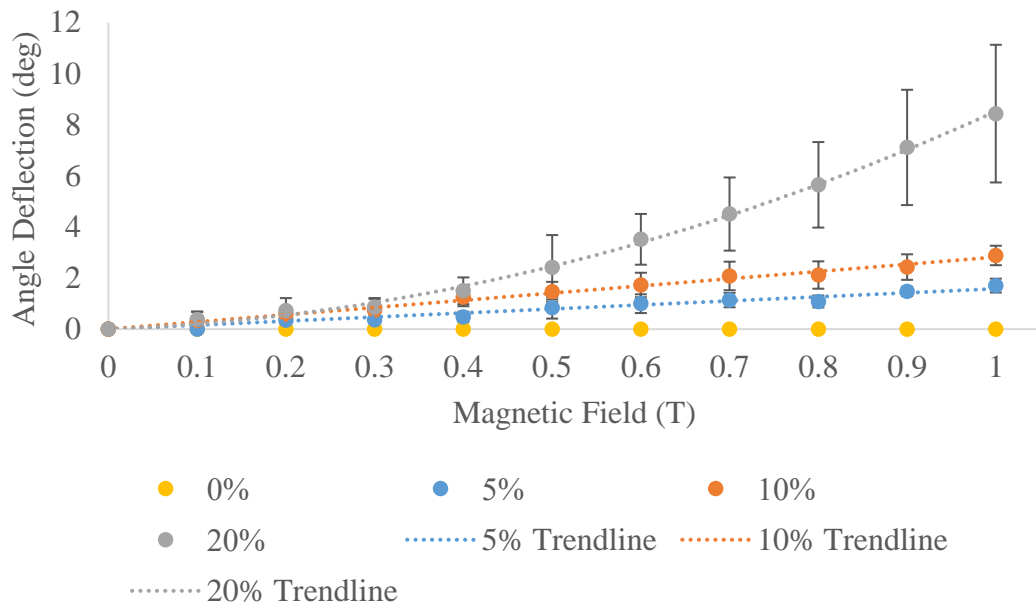
Figure 4.18

Angle Deflection of Aligned Samples with respect to Magnetic Field
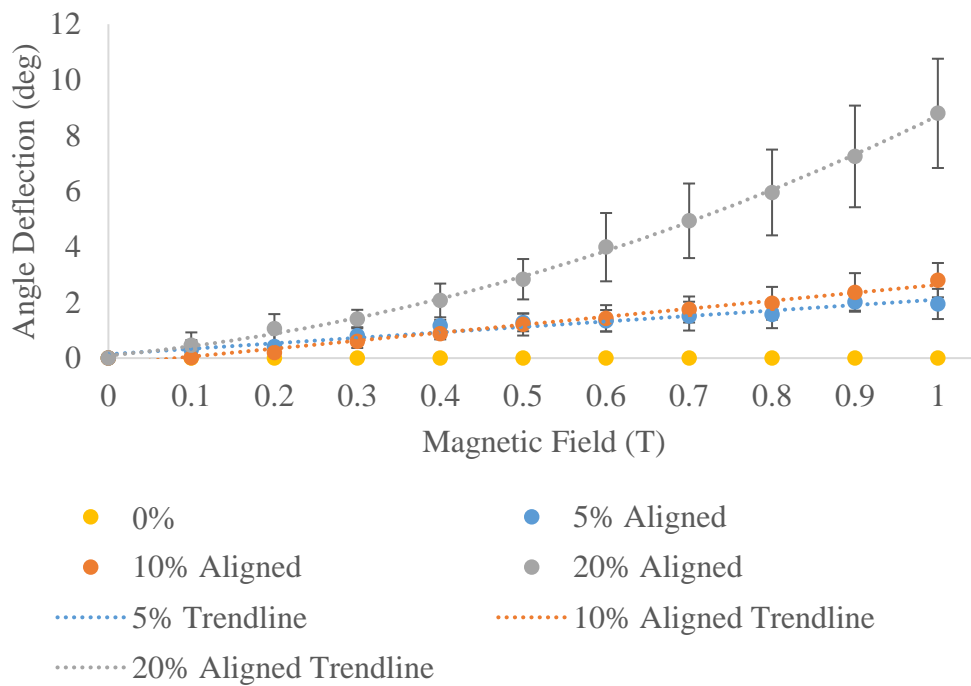
These Figure 4.19, 4.20, and 4.21 show the angle deflection of aligned and non-aligned magnetic films with respect to the magnetic field. The plain PDMS is also included in the graphs to serve as a baseline result.

Looking at the figures, the alignment of the magnetic domains had little to no effect on the angle deflection on all of the concentrations. In the 5% concentration, the alignment did not have an effect on the angle deflection and then the different is every small. Many of the error bars from the standard deviation are overlapping and this shows that the difference of the alignment makes has some significance.

Figure 4.19

Angle Deflection of 5% Concentration Film
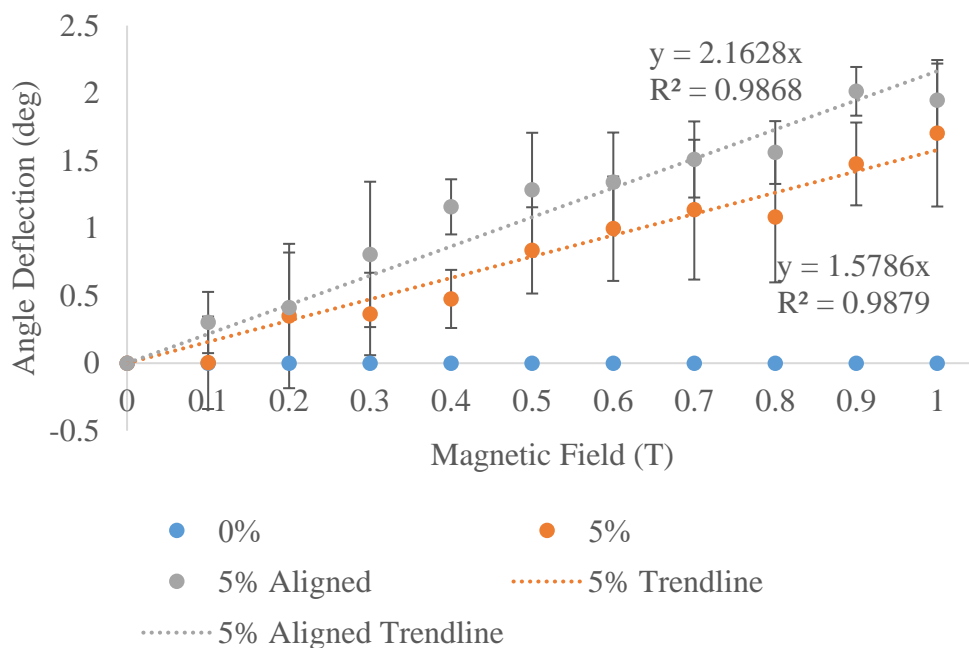
In the 10% concentration condition, the alignment does not seem to have improved the angle deflection as the angle deflection of the non-aligned is overall more than the aligned film. Looking at this case more closely, the 10% non-aligned samples did seem more thinner than the aligned sample and could influence the angle deflection. A lot of the error bars are overlapping, and this hints that the difference between two conditions is not statistically significant.

In the 20% concentration conditions, the aligned samples showed higher angle deflection than the non-aligned samples. Though a difference can be seen at all the points of the graph, the difference is very small and might be negligible like in the 5% and 10% case. The error bars also overlapping which helps to imply that the difference is not significantly different.

Figure 4.20

Angle Deflection of 10% Concentration Film
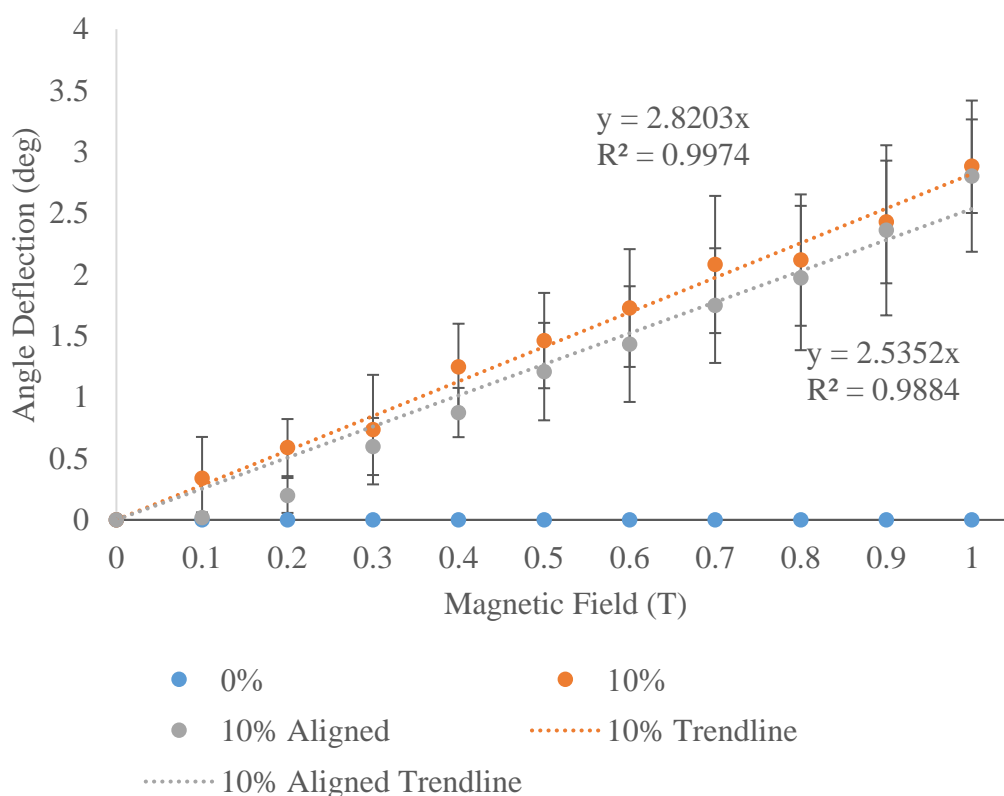
Figure 4.21

Angle Deflection of 20% Concentration Film
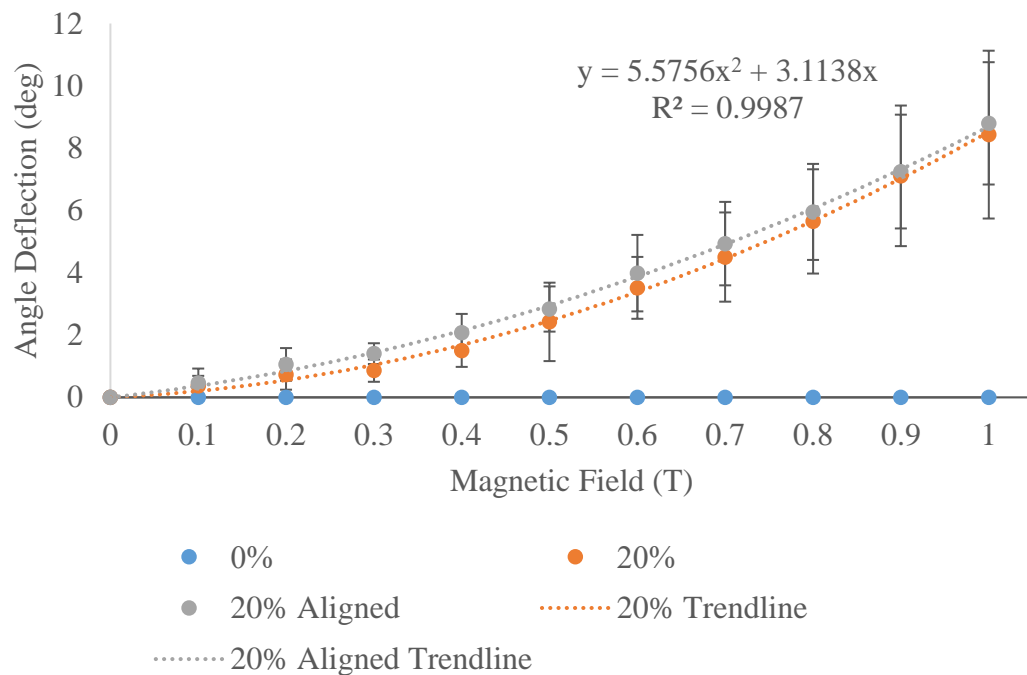
4.2.3 Sensitivity

After the data were plotted in the graphs, the graphs were then used for curve fitting. The curve fitting is used to make a linear relation out of the data from the graph. From the linear relations, we can find the slope of the line in the graph and find the sensitivity of the structures to that magnetic field in each concentration. To check curve fitting with the data, the R squared value can be used to show whether the line that was curve fitted fits the data. A good value of R squared is a value that is close to a value of 1.

The results from the 20% concentration sample had to be handled with special consideration. The results from the graph of this concentration were not linear but matches a second-degree order polynomial. To resolve this case, the data points from 0.3 Tesla to 1 Tesla were only considered for the curve fitting as shown in Figure 4.22. This yielded a more linear relation from the graph.

Figure 4.22

Linear Graph of 20% Concentration Film
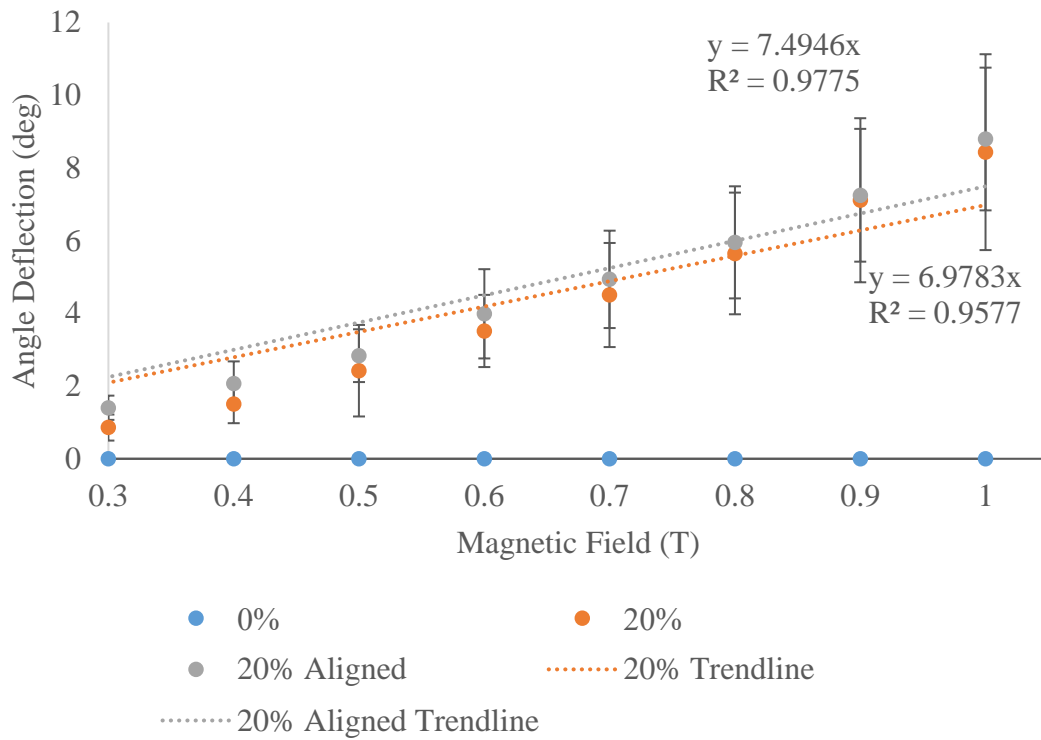
From Table 4.5, the sensitivity of the structure increases with the increase of concentration of nanoparticles. As more nanoparticles are in the nanocomposite, the greater the resultant force when the nanoparticles are magnetized. However, this trend is not consistent in terms of sensitivity of the aligned or non-aligned samples. With the 5% and 10% concentration samples, the sensitivity increases but the difference of sensitivity of the 10% concentration samples is almost negligible. The 20% concentration samples show a decrease with the sensitivity, but the difference is very little.

Table 4.5

Sensitivity with Respect to Concentration and Alignment and R-squared value

Concentration	Sensitivity (deg/T)	R squared
0%	0	
5%	1.579	0.9879
5% Aligned	2.163	0.9868
10%	2.820	0.9974
10% Aligned	2.535	0.9884
20%	6.978	0.9577
20% Aligned	7.495	0.9775

CHAPTER 5
CONCLUSION AND RECOMMENDATIONS

5.1 Restating Objectives

The objectives are restated and will be addressed in this chapter.

Objectives:

1. To develop a magnetic soft structure using magnetic nanoparticles incorporated in polydimethylsiloxane (PDMS) polymer that is flexible and can be deflected using an external magnetic field.

2. To characterize the nanoparticles to analyze the morphological and material properties, and to evaluate the structural integrity and mechanical strength of the magnetic soft structure.

3. To evaluate and demonstrate the movements of the magnetic soft structure under the influence of an externally applied magnetic field and investigate the movement with respect to the concentrations of the magnetic nanoparticles.

For the first objective, we were able to make develop a magnetic soft structure that was embedded with magnetic nanoparticles, which were synthesized in the lab, in the soft structure. The prepared nanoparticles showed an average size of slightly more than 10 nm. These particles were single crystalline showing the (311) plane at the surface. This was further confirmed by XRD.

For the second objective, we were able to do characterization with the transmitted electron microscope (TEM), x-ray powder diffraction, and texture analysis test. The TEM and XRD both showed results that correlates to each very well while the texture analysis text raised some questions. The texture analysis first shows a decreasing trend to from 0 to 10% concentration but increases again at 20% concentration.

For the third objective, we were able to evaluate and demonstrate the movements of the structure by varying the magnetic field by using an electromagnet and varying the current. We evaluated the movement of the structure by analyzing the angle deflection and compared it to the concentration and the alignment of the magnetic domains. The

increasing the concentration also increased the angle deflection of the structure and made the structure more sensitive to the magnetic field. Although the alignment had an effect in the initial testing, it did not show much effect on the angle deflection of the structures as shown in Table 5.1.

Table 5.1

Differences between Non-aligned and Aligned Samples

Concentration	Non-aligned Final Angle Deflection (deg)	Aligned Final Angle Deflection (deg)	Difference
5	1.703	1.947	0.2440
10	2.883	2.802	-0.0810
20	8.434	8.796	0.3620

5.2 Questions from this Study

While working in this study, some of results presented some questions that are left to be answered.

Questions:

1. Why does the 20% concentration magnetic film show a non-linear relationship between the angle deflection and the magnetic field while the other concentrations showed linear relationships?
2. Does the time of the curing factor in the differences in angle deflection?
3. Why did the initial testing show that the alignment had an effect of the angle deflection but not during the experiment?
4. How to control and manipulate the structure without the magnet being in close contact?

These questions must be answered through future works and research.

5.3 Recommendations

When synthesizing the iron oxide nanoparticles, it is crucial that the any water or ethanol that was used to wash the iron oxide nanoparticles be extracted or dried out. When mixing the PDMS with the iron oxide nanoparticles that was not completely

dried, the nanoparticles kept clumping up with each other. The finished iron oxide nanoparticles should have a 'crispy' and dry texture.

The nanoparticles used for this study may have to be a magnetically hard material such as neodymium. These nanoparticles can provide have good magnetization and magnetic tuning. The nanoparticles can be tuned to react to a magnetic field a certain way and change if there is also a change in the magnetic field. This, however, may compromise the biocompatibility of the structure and the application in medicine might be limited.

A system might need to be designed to emit a strong magnetic field at a distance. The problem with electromagnets that was used is that the magnetic field of the electromagnet is very close to the electromagnet. Any magnetic field at a distance from the electromagnet is considered negligible. A suggestion in future research is using a Helmholtz coil which are two big coils with current running through them.

REFERENCES

6.9: Hard and Soft Magnets - Chemistry LibreTexts. (n.d.). Retrieved May 7, 2021, from https://chem.libretexts.org/Bookshelves/Inorganic_Chemistry/Book%3A_Introduction_to_Inorganic_Chemistry/06%3A_Metals_and_Alloys-_Structure_Bonding_Electronic_and_Magnetic_Properties/6.09%3A_Hard_and_Soft_Magnets

Anbarasu, M., Anandan, M., Chinnasamy, E., Gopinath, V., & Balamurugan, K. (2015). Synthesis and characterization of polyethylene glycol (PEG) coated Fe 3O4 nanoparticles by chemical co-precipitation method for biomedical applications. *Spectrochimica Acta - Part A: Molecular and Biomolecular Spectroscopy*, *135*, 536–539. https://doi.org/10.1016/j.saa.2014.07.059

Chen, B., Zhu, Y., Zhao, J., & Cai, H. (2015). Design of a prototype of an adaptive soft robot based on ferrofluid. *2015 IEEE International Conference on Robotics and Biomimetics, IEEE-ROBIO 2015*, 511–516. https://doi.org/10.1109/ROBIO.2015.7418819

Engineers Edge. (n.d.). *Magnetic Lifting Force, Design, Equation and Calculator | Engineers Edge | www.engineersedge.com*. Retrieved April 27, 2021, from https://www.engineersedge.com/calculators/magnet-lifting/magnetic_force_calculator.htm

Hesas, R. H., Baei, M. S., Rostami, H., Gardy, J., & Hassanpour, A. (2019). An investigation on the capability of magnetically separable Fe3O4/mordenite zeolite for refinery oily wastewater purification. *Journal of Environmental Management*, *241*, 525–534. https://doi.org/10.1016/j.jenvman.2018.09.005

Ijaz, S., Li, H., Hoang, M. C., Kim, C. S., Bang, D., Choi, E., & Park, J. O. (2020). Magnetically actuated miniature walking soft robot based on chained magnetic microparticles-embedded elastomer. *Sensors and Actuators, A: Physical*, *301*, 111707. https://doi.org/10.1016/j.sna.2019.111707

Jalil, Z., Rahwanto, A., & Handoko, E. (2017). *Magnetic behavior of natural magnetite (Fe 3 O 4) extracted from beach sand obtained by mechanical alloying method ARTICLES YOU MAY BE INTERESTED IN Synthesis and characterization of black, red and yellow nanoparticles pigments from the iron*

sand AIP Conference Magnetic Behavior of Natural Magnetite (Fe 3 O 4) Extracted from Beach Sand Obtained by Mechanical Alloying Method. *1862*, 165. https://doi.org/10.1063/1.4991127

Kim, J. H., Kang, S. M., Lee, B. J., Ko, H., Bae, W. G., Suh, K. Y., Kwak, M. K., & Jeong, H. E. (2015). Remote Manipulation of Droplets on a Flexible Magnetically Responsive Film. *Scientific Reports*, *5*, 1–10. https://doi.org/10.1038/srep17843

Kim, S., Laschi, C., & Trimmer, B. (2013). Soft robotics: A bioinspired evolution in robotics. *Trends in Biotechnology*, *31*(5), 287–294. https://doi.org/10.1016/j.tibtech.2013.03.002

Lai, C. W., Low, F. W., Tai, M. F., & Abdul Hamid, S. B. (2018). Iron oxide nanoparticles decorated oleic acid for high colloidal stability. *Advances in Polymer Technology*, *37*(6), 1712–1721. https://doi.org/10.1002/adv.21829

Liu, S., Yu, B., Wang, S., Shen, Y., & Cong, H. (2020). Preparation, surface functionalization and application of Fe3O4 magnetic nanoparticles. *Advances in Colloid and Interface Science*, *281*, 102165. https://doi.org/10.1016/j.cis.2020.102165

Mody, V. V., Singh, A., & Wesley, B. (2013). Basics of magnetic nanoparticles for their application in the field of magnetic fluid hyperthermia. In *European Journal of Nanomedicine* (Vol. 5, Issue 1, pp. 11–21). De Gruyter. https://doi.org/10.1515/ejnm-2012-0008

Paknahad, A. A., & Tahmasebipour, M. (2019). An electromagnetic micro-actuator with PDMS-Fe3O4 nanocomposite magnetic membrane. *Microelectronic Engineering*, *216*(March), 111031. https://doi.org/10.1016/j.mee.2019.111031

Shen, L., Li, B., & Qiao, Y. (2018). Fe3O4 nanoparticles in targeted drug/gene delivery systems. In *Materials* (Vol. 11, Issue 2, p. 324). MDPI AG. https://doi.org/10.3390/ma11020324

Sousa, D., Ferreira, D., Rodrigues, J. L., & Rodrigues, L. R. (2019). Nanotechnology in Targeted Drug Delivery and Therapeutics. In *Applications of Targeted Nano Drugs and Delivery Systems*. https://doi.org/10.1016/b978-0-12-814029-1.00014-4

Tong, Y., Liu, X., & Zhang, L. (2019). Green construction of Fe3O4@GC submicrocubes for highly sensitive magnetic dispersive solid-phase extraction of five phthalate esters in beverages and plastic bottles. *Food Chemistry*, *277*, 579–

585. https://doi.org/10.1016/j.foodchem.2018.11.021

Wulandari, I. O., Mardila, V. T., Santjojo, D. J. D. H., & Sabarudin, A. (2018).
Preparation and Characterization of Chitosan-coated Fe3O4 Nanoparticles using
Ex-Situ Co-Precipitation Method and Tripolyphosphate/Sulphate as Dual
Crosslinkers. *IOP Conference Series: Materials Science and Engineering*,
299(1), 012064. https://doi.org/10.1088/1757-899X/299/1/012064

Zhao, R., Kim, Y., Chester, S. A., Sharma, P., & Zhao, X. (2019). Mechanics of hard-
magnetic soft materials. *Journal of the Mechanics and Physics of Solids*, *124*,
244–263. https://doi.org/10.1016/j.jmps.2018.10.008

APPENDIX

FIGURES AND TABLES USED IN PROJECT

Table A1 Angle Deflection of 5% Concentration PDMS with Respect to Magnetic Field

Magnetic Field (T)	Angle Deflection (deg)	Standard Deviation
0	0	0
0.1	0.0032	0.2267
0.2	0.3494	0.4085
0.3	0.3646	0.5383
0.4	0.4760	0.2041
0.5	0.8354	0.4233
0.6	0.9960	0.3673
0.7	1.137	0.2817
0.8	1.082	0.2326
0.9	1.476	0.1803
1.0	1.703	0.2715

Table A2 Angle Deflection of 5% Concentration Aligned PDMS with Respect to Magnetic Field

Magnetic Field (T)	Angle Deflection (deg)	Standard Deviation
0	0	0
0.1	0.3014	0.3424
0.2	0.4110	0.5345
0.3	0.8058	0.3054
0.4	1.158	0.2152
0.5	1.283	0.3193
0.6	1.341	0.3866
0.7	1.509	0.5177
0.8	1.560	0.4833
0.9	2.013	0.3066
1.0	1.947	0.5424

Table A3 *Angle Deflection of 10% Concentration PDMS with Respect to Magnetic Field*

Magnetic Field (T)	Angle Deflection (deg)	Standard Deviation
0	0	0
0.1	0.3378	0.3379
0.2	0.5890	0.2327
0.3	0.7356	0.4465
0.4	1.248	0.3514
0.5	1.461	0.3886
0.6	1.727	0.4801
0.7	2.082	0.5592
0.8	2.118	0.5355
0.9	2.428	0.5000
1.0	2.883	0.3815

Table A4 Angle Deflection of 10% Concentration Aligned PDMS with Respect to Magnetic Field

Magnetic Field (T)	Angle Deflection (deg)	Standard Deviation
0	0	0
0.1	0.01700	0.04320
0.2	0.1988	0.1423
0.3	0.5980	0.2327
0.4	0.8748	0.2007
0.5	1.209	0.3973
0.6	1.433	0.4716
0.7	1.747	0.4675
0.8	1.971	0.5884
0.9	2.360	0.6935
1.0	2.802	0.6165

Table A5 Angle Deflection of 20% Concentration PDMS with Respect to Magnetic Field

Magnetic Field (T)	Angle Deflection (deg)	Standard Deviation
0	0	0
0.1	0.3696	0.3205
0.2	0.7304	0.4841
0.3	0.8582	0.3583
0.4	1.501	0.5231
0.5	2.423	1.259
0.6	3.515	0.9934
0.7	4.504	1.432
0.8	5.648	1.673
0.9	7.111	2.257
1.0	8.434	2.694

Table A6 Angle Deflection of 20% Concentration Aligned PDMS with Respect to Magnetic Field

Magnetic Field (T)	Angle Deflection (deg)	Standard Deviation
0	0	0
0.1	0.4668	0.4576
0.2	1.058	0.5243
0.3	1.403	0.3331
0.4	2.073	0.6058
0.5	2.836	0.7259
0.6	3.988	1.227
0.7	4.935	1.340
0.8	5.953	1.541
0.9	7.248	1.826
1.0	8.796	1.963

Table A7 Angle Deflection of 5% Concentration PDMS with Respect to Current

Current (A)	Angle Deflection (deg)	Standard Deviation
0	0	0
0.070	0.0032	0.2267
0.14	0.3494	0.4085
0.20	0.3646	0.5383
0.27	0.4760	0.2041
0.34	0.8354	0.4233
0.41	0.9960	0.3673
0.47	1.137	0.2817
0.54	1.082	0.2326
0.61	1.476	0.1803
0.68	1.703	0.2715

Table A8 Angle Deflection of 5% Concentration Aligned PDMS with Respect to Current

Current (A)	Angle Deflection (deg)	Standard Deviation
0	0	0
0.070	0.3014	0.3424
0.14	0.4110	0.5345
0.20	0.8058	0.3054
0.27	1.158	0.2152
0.34	1.283	0.3193
0.41	1.341	0.3866
0.47	1.509	0.5177
0.54	1.560	0.4833
0.61	2.013	0.3066
0.68	1.947	0.5424

Table A9 Angle Deflection of 10% Concentration PDMS with Respect to Current

Current (A)	Angle Deflection (deg)	Standard Deviation
0	0	0
0.070	0.3378	0.3379
0.14	0.5890	0.2327
0.20	0.7356	0.4465
0.27	1.248	0.3514
0.34	1.461	0.3886
0.41	1.727	0.4801
0.47	2.082	0.5592
0.54	2.118	0.5355
0.61	2.428	0.5000
0.68	2.883	0.3815

Table A10 Angle Deflection of 10% Concentration Aligned PDMS with Respect to Current

Current (A)	Angle Deflection (deg)	Standard Deviation
0	0	0
0.070	0.01700	0.04320
0.14	0.1988	0.1423
0.20	0.5980	0.2327
0.27	0.8748	0.2007
0.34	1.209	0.3973
0.41	1.433	0.4716
0.47	1.747	0.4675
0.54	1.971	0.5884
0.61	2.360	0.6935
0.68	2.802	0.6165

Table A11 Angle Deflection of 20% Concentration PDMS with Respect to the Current

Current (A)	Angle Deflection (deg)	Standard Deviation
0	0	0
0.070	0.3696	0.3205
0.14	0.7304	0.4841
0.20	0.8582	0.3583
0.27	1.501	0.5231
0.34	2.423	1.259
0.41	3.515	0.9934
0.47	4.504	1.432
0.54	5.648	1.673
0.61	7.111	2.257
0.68	8.434	2.694

Table A12 Angle Deflection of 20% Concentration Aligned PDMS with Respect to Current

Current (A)	Angle Deflection (deg)	Standard Deviation
0	0	0
0.070	0.4668	0.4576
0.14	1.058	0.5243
0.20	1.403	0.3331
0.27	2.073	0.6058
0.34	2.836	0.7259
0.41	3.988	1.227
0.47	4.935	1.340
0.54	5.953	1.541
0.61	7.248	1.826
0.68	8.796	1.963

Table A13 Specification of XP34/25 Electromagnet

Specification	
Model Number	P34/25
Holding Force	25 kg
Input Voltage	12V
Dimension	34x20mm
Weight	130g

Table A14 Specification of MK-P34/25 Electromagnet

Specification	
Model Number	MK-P34/25
Input Voltage	12V
Current	0.5A
Power Consumption	6W
Holding Force	20kg
Dimension	34x25mm
Weight	137g

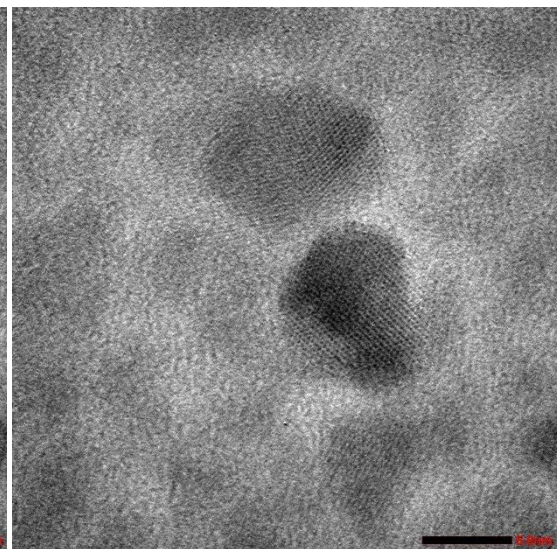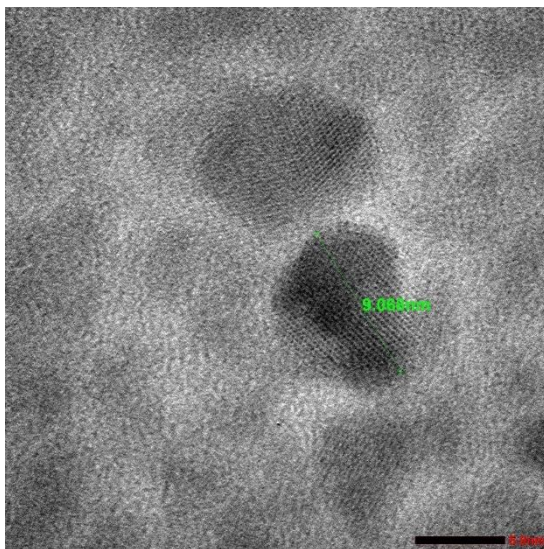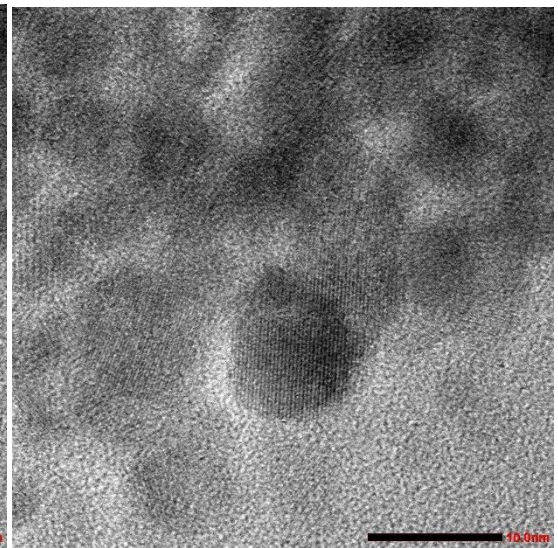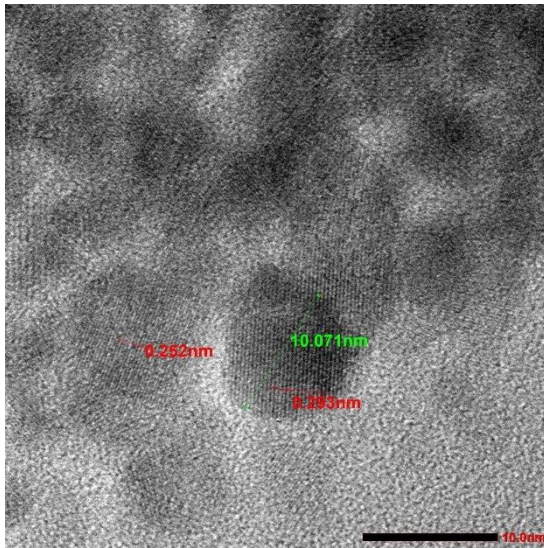**Figure A1 TEM Images of Fe₂O₃ magnetic nanoparticles.**
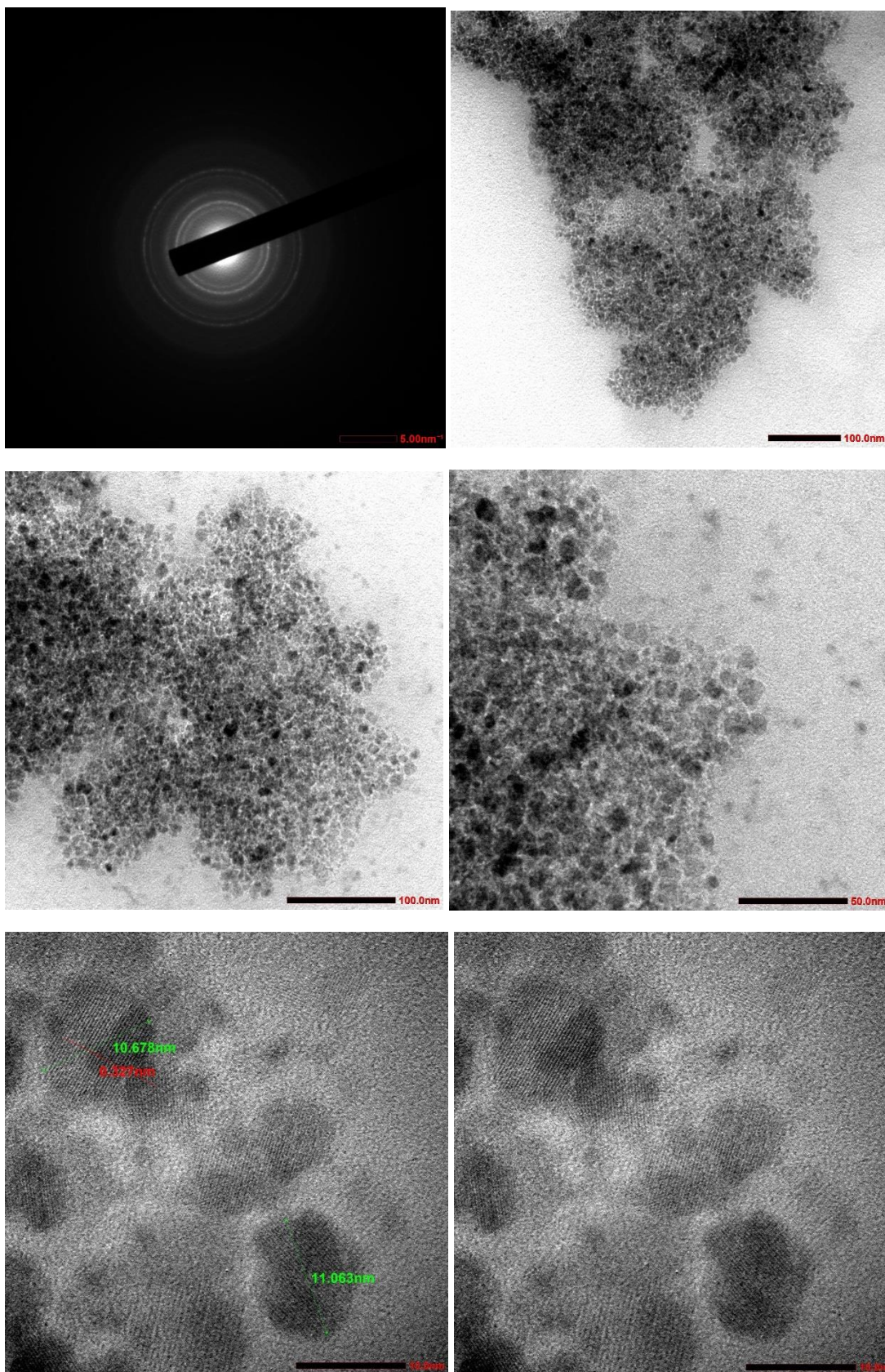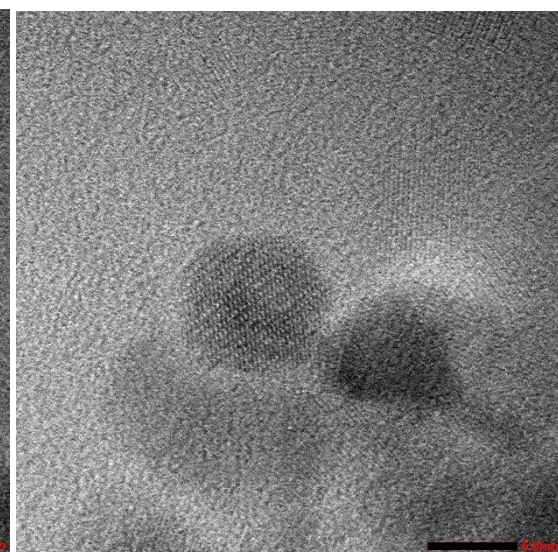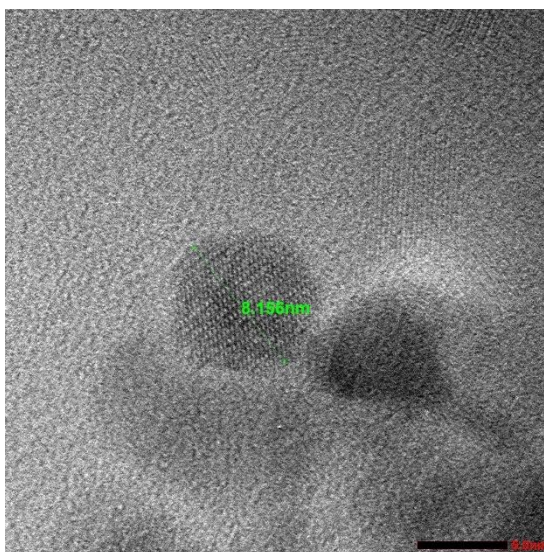
Figure A2 Results from Texture Analysis Test of 0% Concentration PDMS

Job number	64-U04-2423	Sample number	2100424-2100426
Sample name	PDMS	Operator	Anantaya L.
Report Date	19/4/2564	Test Date	19/4/2564
Temperature	22.8	Humidity:	50.1
Testing Machine	EZ-X	Machine No.	I30835735007
Capacity	50N	Test Mode	Single
Test Type	Tensile	Speed	25mm/min

Name Parameters Unit	Max_Force Calc. at Entire Areas N	Max_Disp. Calc. at Entire Areas mm	Max_Stress Calc. at Entire Areas MPa	Max_Strain Calc. at Entire Areas %
Thin Film PDMS 0 % _1	8.19617	25.4055	0.54641	97.7135
Thin Film PDMS 0 % _2	9.35912	22.3941	0.62394	86.1313
Thin Film PDMS 0 % _3	8.26065	22.7525	0.55071	87.5096
Average	8.60531	23.5174	0.57369	90.4515
Standard Deviation	0.65361	1.64496	0.04357	6.32675

Name Parameters Unit	Elastic Force 0.1 - 0.2 N MPa	Thickness mm	Width mm	Gauge_Length mm
Thin Film PDMS 0 % _1	0.76329	1.0000	15.0000	26.0000
Thin Film PDMS 0 % _2	1.02430	1.0000	15.0000	26.0000
Thin Film PDMS 0 % _3	0.95567	1.0000	15.0000	26.0000
Average	0.91442	1.0000	15.0000	26.0000
Standard Deviation	0.13531	0.00000	0.00000	0.00000

Figure A3 Results from Texture Analysis Test of 5% Concentration PDMS

Job number	64−U04−2423	Sample number	2100427−2100429
Sample name	PDMS 5% IONP	Operator	Anantaya L.
Report Date	19/4/2564	Test Date	19/4/2564
Temperature	22.8	Humidity:	50.1
Testing Machine	EZ−X	Machine No.	I30835735007
Capacity	50N	Test Mode	Single
Test Type	Tensile	Speed	25mm/min

Name Parameters Unit	Max_Force Calc. at Entire Areas N	Max_Disp. Calc. at Entire Areas mm	Max_Stress Calc. at Entire Areas MPa	Max_Strain Calc. at Entire Areas %
Thin Film PDMS−IONP 5 % _ 1	3.79789	25.7054	0.25319	98.8668
Thin Film PDMS−IONP 5 % _ 2	3.37405	28.1174	0.22494	108.144
Thin Film PDMS−IONP 5 % _ 3	3.06652	28.5853	0.20443	109.943
Average	3.41282	27.4694	0.22752	105.651
Standard Deviation	0.36722	1.54545	0.02448	5.94398

Name Parameters Unit	Elastic Force 0.1 − 0.2 N MPa	Thickness mm	Width mm	Gauge_Length mm
Thin Film PDMS−IONP 5 % _ 1	0.43089	1.0000	15.0000	26.0000
Thin Film PDMS−IONP 5 % _ 2	0.35356	1.0000	15.0000	26.0000
Thin Film PDMS−IONP 5 % _ 3	0.31044	1.0000	15.0000	26.0000
Average	0.36496	1.0000	15.0000	26.0000
Standard Deviation	0.06103	0.00000	0.00000	0.00000

Figure A4 Results from Texture Analysis Test of 10% Concentration PDMS

Job number	64–U04–2423	Sample number	2100430–2100432
Sample name	PDMS 10% IONP	Operator	Anantaya L.
Report Date	19/4/2564	Test Date	19/4/2564
Temperature	22.8	Humidity:	50.1
Testing Machine	EZ–X	Machine No.	I30835735007
Capacity	50N	Test Mode	Single
Test Type	Tensile	Speed	25mm/min

Name Parameters Unit	Max_Force Calc. at Entire Areas N	Max_Disp. Calc. at Entire Areas mm	Max_Stress Calc. at Entire Areas MPa	Max_Strain Calc. at Entire Areas %
Thin Film PDMS–IONP 10 % _ 1	1.72959	24.8696	0.11531	95.6524
Thin Film PDMS–IONP 10 % _ 2	1.45582	22.1641	0.09705	85.2466
Thin Film PDMS–IONP 10 % _ 3	1.98914	25.0011	0.13261	96.1582
Average	1.72485	24.0116	0.11499	92.3524
Standard Deviation	0.26669	1.60133	0.01778	6.15900

Name Parameters Unit	Elastic Force 0.1 – 0.2 N MPa	Thickness mm	Width mm	Gauge_Length mm
Thin Film PDMS–IONP 10 % _ 1	0.19644	1.0000	15.0000	26.0000
Thin Film PDMS–IONP 10 % _ 2	0.17298	1.0000	15.0000	26.0000
Thin Film PDMS–IONP 10 % _ 3	0.22562	1.0000	15.0000	26.0000
Average	0.19835	1.0000	15.0000	26.0000
Standard Deviation	0.02637	0.00000	0.00000	0.00000

**Figure A5 Results from Texture Analysis Test of 20% Concentration PDMS**

Job number	64-U04-2423	Sample number	2100433-2100435
Sample name	PDMS 20% IONP	Operator	Anantaya L.
Report Date	19/4/2564	Test Date	19/4/2564
Temperature	22.8	Humidity:	50.1
Testing Machine	EZ-X	Machine No.	I30835735007
Capacity	50N	Test Mode	Single
Test Type	Tensile	Speed	25mm/min

Name Parameters Unit	Max_Force Calc. at Entire Areas N	Max_Disp. Calc. at Entire Areas mm	Max_Stress Calc. at Entire Areas MPa	Max_Strain Calc. at Entire Areas %
Thin Film PDMS-IONP 20 %_1	2.99155	32.1761	0.19944	123.754
Thin Film PDMS-IONP 20 %_2	1.53602	27.3051	0.10240	105.020
Thin Film PDMS-IONP 20 %_3	4.05012	40.9034	0.27001	157.321
Average	2.85923	33.4615	0.19062	128.698
Standard Deviation	1.26226	6.88968	0.08415	26.4987

Name Parameters Unit	Elastic Force 0.1 - 0.2 N MPa	Thickness mm	Width mm	Gauge_Length mm
Thin Film PDMS-IONP 20 %_1	0.30613	1.0000	15.0000	26.0000
Thin Film PDMS-IONP 20 %_2	0.13717	1.0000	15.0000	26.0000
Thin Film PDMS-IONP 20 %_3	0.35018	1.0000	15.0000	26.0000
Average	0.26449	1.0000	15.0000	26.0000
Standard Deviation	0.11244	0.00000	0.00000	0.00000

Figure A6 Angle Deflection of 0% Concentration PDMS
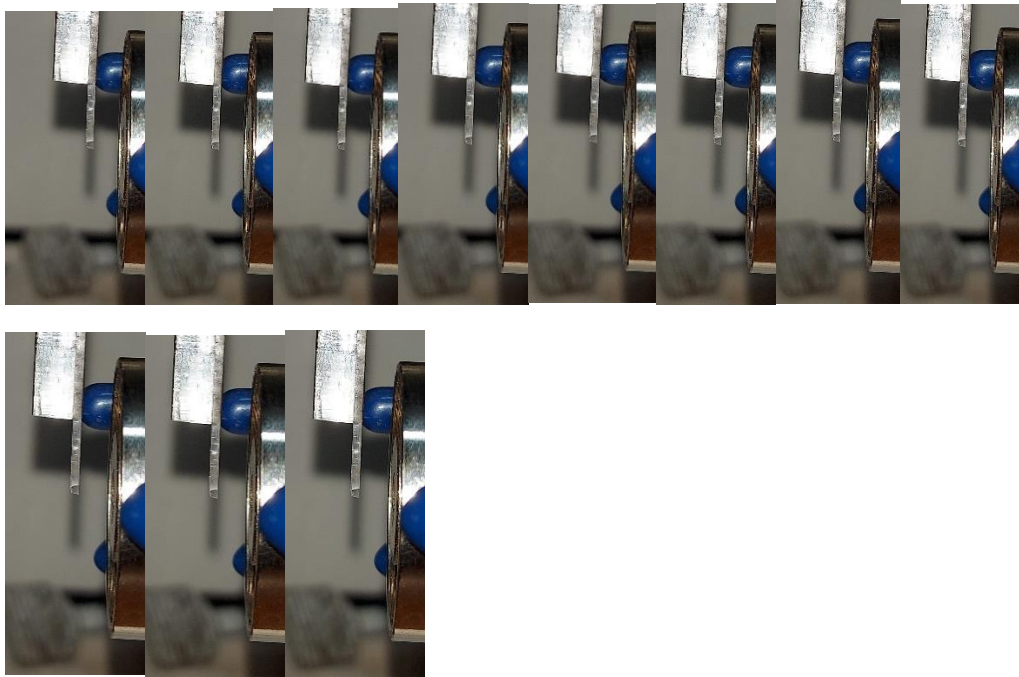
Note. (0 to 1 Tesla at an increment of 0.1 Tesla from left to right)

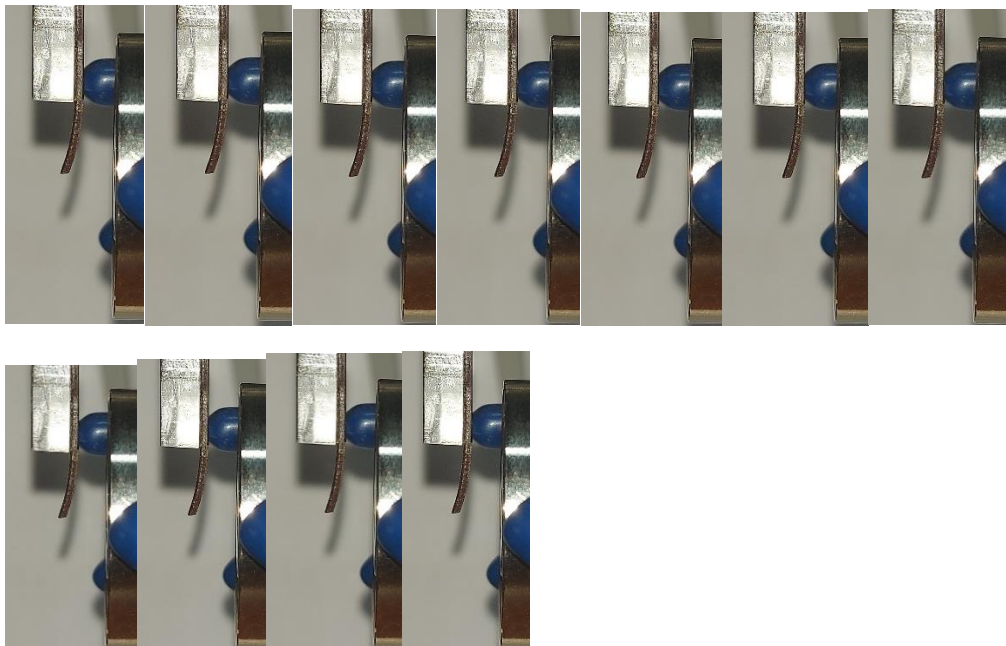**Figure A7 Angle Deflection of 5% Concentration PDMS**
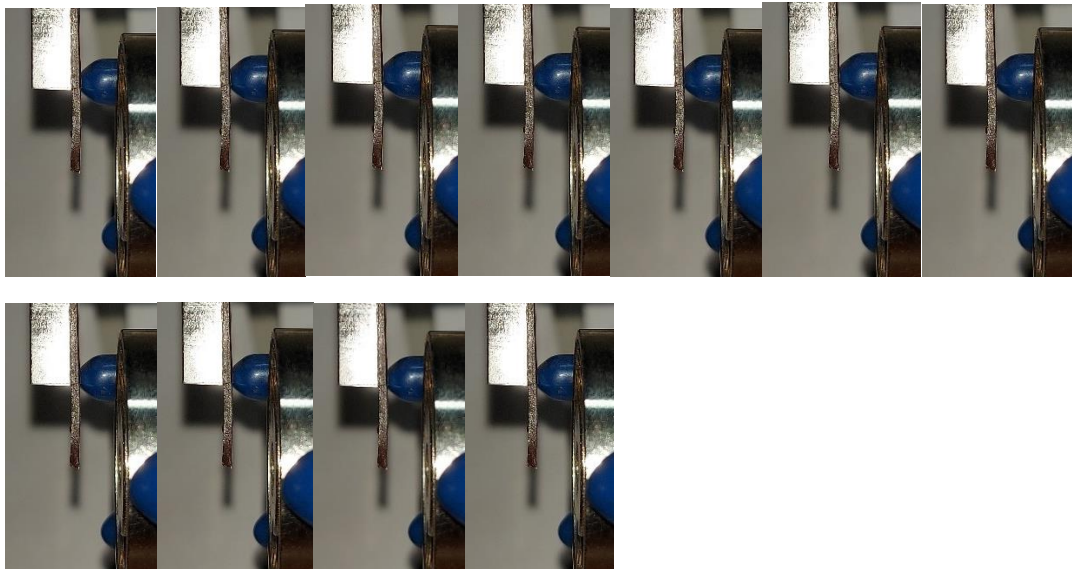
Note. (0 to 1 Tesla at an increment of 0.1 Tesla from left to right)

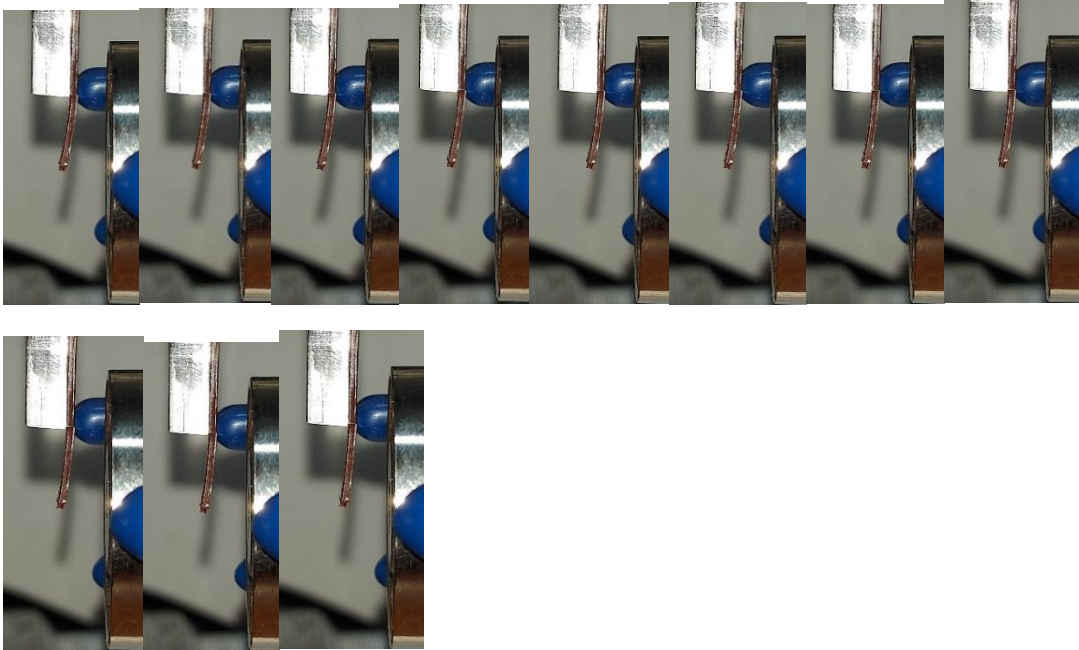**Figure A8 Angle Deflection of 5% Concentration Aligned PDMS**

Note. (0 to 1 Tesla at an increment of 0.1 Tesla from left to right)

Figure A9 Angle Deflection of 10% Concentration PDMS
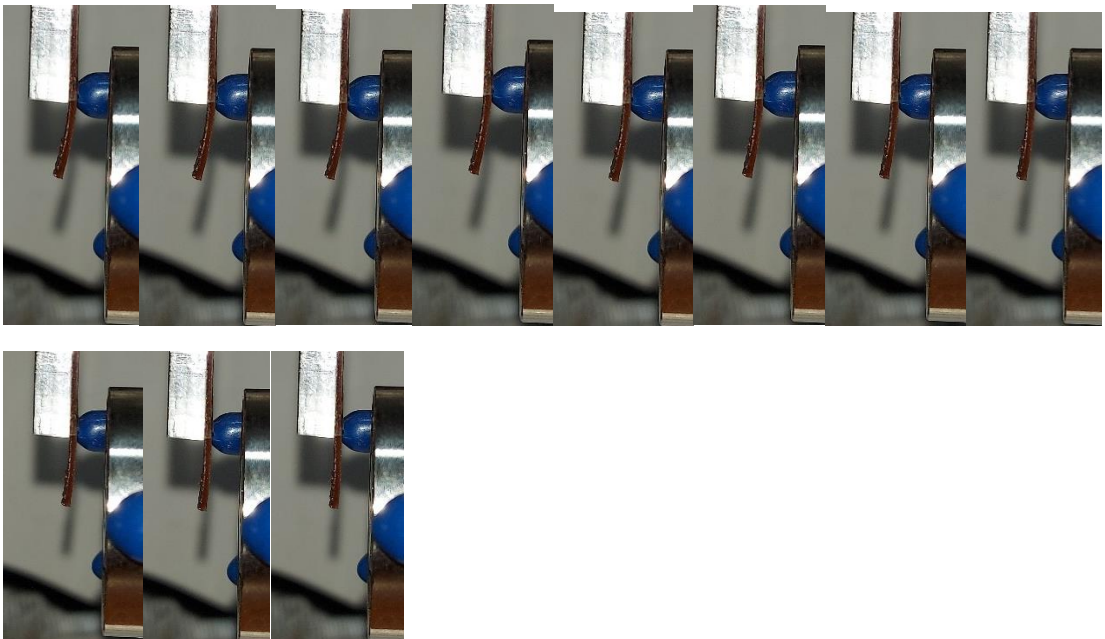

Note. (0 to 1 Tesla at an increment of 0.1 Tesla from left to right)

Figure A10 Angle Deflection of 10% Concentration Aligned PDMS

Note. (0 to 1 Tesla at an increment of 0.1 Tesla from left to right)

Figure A11 Angle Deflection of 20% Concentration PDMS

Note. (0 to 1 Tesla at an increment of 0.1 Tesla from left to right)

Figure A12 Angle Deflection of 20% Concentration Aligned PDMS

Note. (0 to 1 Tesla at an increment of 0.1 Tesla from left to right)

Figure A13 Image of XP 34/25

VITA

Benjamin Dopphoopha was born in Macao, China, on June 2, 1997. He has attended elementary school in Macao in the Macao Anglican College and one year of middle school in Columbia, South Carolina. He continued in online school in Thailand with Southern Baptist Academy and got a diploma by taking the General Educational Development (GED) Test. In August 2015, he entered Chiang Mai University and in August 2019 received the degree of Bachelor of Engineering in Mechanical Engineering with First Class Honors. In the following August, he entered Asian Institute of Technology under His Majesty the King's Scholarship and received a Master of Engineering in Nanotechnology in 2021.